The influence of long-wavelength tilting and climatic change on sediment accumulation

J.J. Armitage (1, 2), R.A. Duller (3) and S.M. Schmalholz (4)

(1) Dynamique des Fluids Géologiques, Univ Paris Diderot, Sorbonne Paris Cité, Institut de Physique du Globe de Paris, UMR 7154 CNRS, F-75013 Paris, France

(2) Department of Earth Science, Royal Holloway, University of London, Egham, Surrey, TW20 0EX, UK

(3) Department of Earth, Ocean and Ecological Sciences, School of Environmental Sciences, University of Liverpool, 4 Brownlow Street, Liverpool L69 3GP, UK

(4) Insititute of Earth Sciences, Faculté des géosciences et de l'environment, Université de Lausanne, Lausanne, Switzerland

Abstract

The elevation of continental interiors over time is demonstrably variable. A major part of change in elevation within the continental interior is likely driven by density changes within the upper mantle and by global mantle convection. For example, upper mantle flow has been invoked as the cause of Neogene uplift of the interior Rocky Mountains and Colorado Plateau, warping and tilting sediment transport slopes that link to the widespread deposition of gravel units within the Great Plains. These geomorphic and sedimentologic features however can also be generated by an increase in run-off, since erosion will promote change in elevation due to isostatic compensation and the loading of the lithosphere by the deposition of sediment. To explore the consequences of change in topography and climate we use a general length dependent diffusive sediment transport law to model both erosion and deposition that includes the concentrative effects of river systems. The simplicity of the approach means that we can collapse sediment transport to one dimension and couple erosion and deposition with plate flexure. We find that for a landscape that is gently tilted (slope of order of 10^{-3}) a change in run-off has a minor effect on transport gradient, as sediment transport and associated flexural response maintain topography at a similar elevation. However, there can be a significant change in depositional style when the degree of tilt is altered by, for example, a local change in upper mantle density. An increase in buoyancy within the upper mantle, which increases slopes, leads to a transient reduction in grain-sizes deposited at a fixed location. This behavior is due to a temporary retreat of the zone of erosion into the catchment

and a transient increase in accommodation space relative to sediment supply. A reduction in tilt has the opposite effect, the older deposits are eroded and the erosion-deposition transition rapidly moves down-system. There is convincing evidence that the formation of thin and laterally extensive conglomeratic units of the Great Plains is due to a reduced rate of subsidence. Based on the results of our coupled model, we suggest that widespread conglomeratic units within the continental interior are in general a consequence of a reduction in slope as the dynamic support for regions of high topography reduces.

1 Introduction

Sediment accumulation within the continental interior and at the passive margins is unsteady and non-uniform, as highlighted by change in sedimentary facies, the caliber of deposits (e.g. gravels, sands and silts), and by change in sediment accumulation rates. In some cases these changes can be linked to clear tectonic or climatic events that affected regional topography or sediment flux, while decoding the reason for change in other records is not so clear (Armitage et al., 2011). For example the Zambezi Delta succession records an increase in sediment delivery from the Oligocene until the Quaternary (Walford et al., 2005). This change in sediment accumulation has been associated with: the onset of extension in the East African Rift; regional uplift and tilting due to a deep thermal anomaly; and drainage reorganization of the Zambezi River catchment (Walford et al., 2005).

In North America the New Jersey Margin experienced a notable increase in sediment accumulation during the Miocene (Poag and Sevon, 1989; Mountain et al., 2007). The reasons for this increase in sediment accumulation are less clear, but there is evidence of coeval rejuvenated erosion within the Appalachian catchments (Gallen et al., 2013; Boettcher and Milliken, 1994), which could be related to regional uplift driven by mantle flow (e.g. Spasojevic et al., 2008). However, an increase in surface run-off during the Miocene due to regional climate change could also lead to increased erosion and sediment delivery to the New Jersey margin. There is also ongoing debate about the mechanism of deposition of widespread gravel units during the Miocene – Pliocene within the Great Plains, United States of America; whether these units signify a change in erosion and deposition due to climatic shifts (Wobus et al., 2010, Tucker & van der Beek, 2013); are linked to long-wavelength tilting of the continental interior (McMillan et al., 2006; Duller et al., 2012); or represent a change in threshold slope due to an autogenic change in run-off (Engelder & Pelletier, 2013).

The widespread deposition of a coarse conglomerate unit within the Spanish Pyrenees during

the Paleocene-Eocene transition is temporally-linked to an increase in surface run-off driven by an abrupt change in climate (Schmitz and Pujalte, 2007; Armitage et al., 2011; Manners et al., 2013). This raises the possibility that similar deposits of laterally extensive gravel sheets are a signature of change in run-off. However, in northwestern America the deposition of gravel units throughout the Cretaceous and Cenozoic have been causally linked to changes in patterns of uplift and subsidence (Heller et al., 2013). Going back further into the geological history of North America, change in the Sloss sequences (Sloss, 1963) within the North American continental platform have been linked to large scale tilting and subsidence due to large-scale mantle anomalies, which are likely a consequence of subduction (Mitrovica et al., 1989; Coakley and Gurnis, 1995; Burgess and Gurnis, 1995).

The key issue that hinders our attempts to accurately decode the cause of observed increases in denudation and sediment accumulation is that both can be a function of change in climate, and the same change in denudation and accumulation could be caused by tectonically or buoyancy-induced changes in surface uplift.

Erosion of bedrock by flowing water is driven by detachment of rock when river systems are incising and there is no alluvial cover. The CONUS soil data set of Miller and White (1998) for the United States of America would suggest that large regions of the continental interior are effectively covered in a transportable regolith. We could therefore infer that on a gross scale erosion is not governed by bedrock-detachment, but the transport of this regolith. Pelletier (2011) uses the CONUS data set of Millar and White (1998) to make a preliminary estimate of the relative importance of erosion by bedrock-detachment and sediment/regolith transport. This work proposed that erosion becomes increasingly limited by the transport of sediment as relief increases (Pelletier, 2011). This inference is contentious however, as it is also the case that the depth to bedrock reduces as elevation increases (Millar and White, 1998). Furthermore, bedrock incision is not uniform through time, as sediment cover will inhibit or drive incision (Sklar and Dietrich, 2001). This leaves the open question: can we assume that erosion at a large spatial and temporal scale is limited by the transport of sediment?

Over days to thousands of years it is arguable that individual events, storms and rapidly fluctuating climate must be considered, as the alluvial cover will change how erosion operates (e.g. Lague et al., 2010). Deposition of widespread conglomerate units such as the Miocene Ogallala Formation within the Great Plains, and change in sediment accumulation at a passive margin, however occur over durations of more than a million years (e.g. Walford et al., 2005; Cather et al., 2012). A package of stratigraphy that represents a million or more years of

deposition holds information about thousands of storm events, as sediment or as time-gaps. In essence, when viewed over geological time scales, it is arguable that the multiple individual storm events become averaged out (Paola et al., 1992). Furthermore, over such long time scales there is evidence that sediment transport across sedimentary systems is buffered to periodic changes in run-off, but is sensitive to shifts to new climatic or tectonic regimes that last for millions of years (Métivier and Gaudemer, 1999; Blum and Tronvisk, 2000; Casteltort and van den Dreissch, 2003). We will therefore focus on exploring how the coupled system responds to a single shift in surface run-off and upper mantle density.

Our aim is to model erosion and deposition along the length of an ancient sediment routing system such as the Ogallala Formation, which starts at the Laramie Range, Wyoming, United States of America, and spreads out onto the Nebraskan Great Plains. Given that the majority of such a low slope sedimentary system traverses a landscape that is covered in transportable sediment or regolith, as for example in the present day Great Plains (Millar and White, 1998), we will assume that erosion and deposition are controlled by the transport of sediment. We build on the work of Smith and Bretherton (1972), Flemings and Jourdan (1989) and Paola et al. (1992) to develop a coupled model of sediment transport with lithosphere flexure. In the early 70's Terence Smith and Francis Bretherton published a mathematical framework showing how a model of sediment flux dependent erosion can recreate realistic morphologies. Two decades later an early model that coupled deposition and flexure was published where sediment transport was assumed to be a linear function of slope (Flemings and Jourdan, 1989). Three years later Chris Paola published a derivation for the conservation of mass for transport within braided alluvial channels and alluvial fans. The derived diffusion equation is referred to as Exner's equation of conservation of bed sediment, after Felix Exner (e.g. Exner, 1920; Paola et al., 1992). In deriving the equations for the change in elevation it was shown that diffusion coefficient is a function of run-off (Paola et al., 1992).

In this article we will first present the model equations for sediment transport, grain size fining, and flexure of the lithosphere. We wish to explore how a landscape will respond to a change in regional topography due to upper mantle flow, and to a change in surface run-off. To model a change in topography driven by a density change in the upper mantle we introduce a positive (upwards) load on the elastically defined lithosphere. This is a simplified representation of the dynamic support that is believed to be responsible for anomalously elevated mountainous regions of the continental interiors, such as the eastern Rocky Mountains in Wyoming and Colorado (Karlstrom et al., 2012).

We will run three different experiments on the coupled system. First, we will create an

elevated region by introducing a permanent density anomaly below the elastically defined lithosphere. Second, we will increase and decrease surface run-off within the model domain by increasing the imposed precipitation rate after a 10 Myr period of model evolution. Third, we will increase and decrease the density of the anomaly driving topographic change in the model after 10 Myr period of model evolution. A 10 Myr initial duration has been chosen on the basis that it is of a similar order of magnitude to the observed periods between change in sediment accumulation within the continental interior and at the continental margins (e.g. Cather et al., 2012). The results of this study will be compared to the record of sediment accumulation across the Great Plains during Miocene – Pliocene times.

2 Methods

2.1 Sediment Transport

Following Dietrich et al. (2003), we begin with a simple idealized landscape composed of bedrock, thickness η (units of m), and a surface layer, regolith, of thickness h (units of m, see Figure 1). This landscape is forced externally through uplift or subsidence, U (units of myr^{-1}). Bedrock is transferred into regolith at a rate, P (myr^{-1}), and regolith is transported across the system with a sediment flux, q_s (m^{2}yr^{-1}). Assuming that the density of regolith produced and transported is equal to the bed rock, within this simple system the rate of change in bedrock thickness is,

$$\partial_t \eta = U - P \quad (1)$$

and the rate of change in regolith thickness is,

$$\partial_t h = P - \partial_x q_s \quad (2)$$

It then follows that the rate of change in landscape elevation is the sum of the two rates of change,

$$\partial_t z = \partial_t \eta + \partial_t h \quad (3)$$

To solve for the change in surface elevation we must make a further assumption. One assumption is that the thickness of the regolith remains roughly constant through geological time, $\partial_t h \sim 0$. This is the equivalent to assuming that any newly generated regolith is instantaneously transported out of the model domain. This leads to the rate of change in landscape elevation being,

$$\partial_t z = U - P \quad (4)$$

The production of regolith becomes a key consideration when modeling regions where rivers are incising into bedrock and also for exploring soil production and weathering. Yet from studies of the thickness of present day regolith across the United States of America (Millar and White, 1998) and assuming that this is representative of most regions of low relief within the continents, it is plausible that there is a supply of transportable regolith is readily available along the majority of the sediment routing system. We make such an assumption and to solve for the change in landscape we carry through the summation in equation 3, assuming the density of transported material is equal to that deposited:

$$\partial_t z = U - \partial_x q_s \quad (5)$$

Equation 5 is a form of the Exner continuity for mass. Using this type of continuity equation and following the derivation of Paola et al, (1992), the change in elevation with time can then be solved by a diffusive equation of the form,

$$\partial_t z = U + \partial_x \left(\nu(q_w) \partial_x z \right) \quad (6)$$

Where the sediment flux is a function of local slope and the diffusion coefficient v is dependent on the water flux, q_w (m^2yr^{-1}, all symbols are listed in Table 1). Assuming that bed-load is transported following the empirical Meyer-Peter – Muller transport laws (Meyer-Peter and Muller, 1984), then the diffusion coefficient is given by (Paola et al., 1992),

$$\nu(q_s) = \frac{8A\left(C_f\right)^{1/2}}{C_0\left(s-1\right)} q_w \quad (7)$$

Where the constant $A = 1$ for the case of a meandering river in an alluvial plain and $A = 0.15$ for a braided river. $C_f = 0.01$ is a dimensionless drag coefficient, $C_0 = 0.7$ is the volume concentration of sediment in the bed and $s = 2.7$ is the sediment specific gravity. Using these values, the diffusion coefficient is given by $v = 0.10q_w$ in the meandering case and $\nu = 0.67q_w$ for the braided case. Using a grain-size dependent critical Shields stress rather than the Meyer-Peter – Muller bed-load transport law, a similar form of the diffusion coefficient (equation 7) was arrived at by Marr et al. (2000) for gravel and sand, giving values of the order of $v = 0.1q_w$ for gravel and $v = 1.0q_w$ for sand. Assuming a catchment length of 100 km and a precipitation rate of 1 myr^{-1}, the diffusion coefficient at the catchment outlet can be estimated to be 10^4 - 10^5 m^2yr^{-1}.

In classic models of foreland basin stratigraphic development it has been assumed that this diffusion coefficient is constant with length down the system, with v = 100 to 5000 m^2yr^{-1}

(Flemings and Jordan, 1989; Sinclair et al., 1991). Depending on the boundary conditions, this simple relationship would lead to rounded or convex up 1-D profiles (Métivier, 1999). Taking a constant diffusion coefficient that is uniform in space is appealing, given its simplicity, yet it does not allow for a change erosion and deposition due to change in water flux down the length of the catchment.

Here we formulate a model for sediment transport that allows for the run-off to increase down the length of the system, as greater quantities of water will be captured within the fluvial network. Following the work of Smith and Bretherton (1972), we assume that sediment flux is a function of both the slope and the surface run-off,

$$\partial_t z = U + \partial_x \left[\left(\kappa + c q_w \right) \partial_x z \right] \tag{8}$$

where c is a constant value that is similar to the product of the constants in equation 7. This relationship states that sediment transport is the sum of a part that is a constant function of slope and a second term that accounts for the increasing water flow down system. This relationship for sediment flux is similar to that proposed by Smith and Bretherton (1972), however we have assumed that there is no power relationship between sediment flux and water flux, and between sediment flux and slope, i.e. $q_s \propto q_w^n \left(\partial_x z \right)^m$, where $n = 1$ and $m = 1$. The exponents n and m are dependent on which model of bed-load transport is thought representative of the large scale transport, for example Einstein – Brown bed-load transport laws give $n = 2$ and $m = 2$, or Meyer-Peter – Muller bed-load transport laws give $n \sim 1$ and $m \sim 1$ (Smith and Bretherton, 1972; Wobus et al., 2010). We have chosen to set $n = 1$ and $m = 1$, not because we believe the Meyer-Peter – Muller bed-load transport laws to be more representative of long-term sediment transport, but to make the system equation simpler, such that sediment flux is simply a function of slope and water flux.

The water flux is found assuming a spatially uniform distribution of precipitation rate, α and then calculating the downhill flow path distance (see Smith and Bretherton, 1972 and Simpson and Schlunneger, 2003),

$$\partial_x \left(\frac{\partial_x z}{|\partial_x z|} q_w \right) = -\alpha \tag{9}$$

The combination of equations 8 and 9 leads to a dominantly diffusive equation, where the effective diffusion coefficient is a function of space and increases down-system.

In these equations for sediment transport we do not make the distinction between the region of the landscape that is eroding and that which is undergoing deposition. Equations 8 and 9

have been used to model the erosion of upland catchments for 1-D models of normal fault bound catchment-fan systems (Densmore et al., 2007; Armitage et al., 2011; 2013) and 2-D models of wedge shape initial topographies (Simpson and Schlunneger, 2003). In the 1-D catchment - fan models, deposition within the sedimentary fan was calculated from a geometric mass balance where there is a continuity of slope between the catchment and fan, at the fan head. However, these equations can equally apply to the alluvial plain and alluvial fans (e.g. Paola et al., 1992; Granjeon and Joseph, 1999). Therefore, to model both erosion and deposition within the continental interior where there is typically a transportable regolith we propose that this transport-limited setup is reasonable.

2.2 Flexure

The vertical displacement of the continental lithosphere can be described by the displacement of an elastic to visco-elastic layer depending on the time scale of observation (Watts et al., 1982; Willett et al., 1985). To understand the first order response to loading and unloading upon the distribution of sediment we treat the upper continental lithosphere as an elastic beam of a preset elastic thickness, as the relaxation time-scale of continental lithosphere is of the order of a few thousand years (Mitrovica and Forte, 1997) and foreland basin architecture can be adequately reproduced by a model of elastic flexure (Flemings and Jordan, 1990). The displacement, w, of the beam due to loading is then simply given by the fourth order differential equation,

$$D_f \partial_x^4 w = p_i - \rho_m g w + \rho_{fill} g \Delta z \qquad (10)$$

Where D_f is the flexural rigidity, p_i is the positive (upwards) load imposed to simulate uplift due to a density anomaly in the mantle, ρ_m is the mantle density, ρ_{fill} is the density of material eroded and deposited, g is the acceleration due to gravity and Δz is the change in elevation due to erosion and deposition. We have assumed that the density of what is eroded is equal to that which is deposited. This is therefore assuming no mass is lost to the system through a process such as chemical weathering and the removal of minerals to the ocean. This is therefore an upper estimate for the deposited load exerted on the lithosphere. The flexural rigidity is given by,

$$D_f = \frac{E T_e^3}{12\left(1-\nu_P^2\right)} \qquad (11)$$

where E is Young's modulus, υ_P is Poisson's ratio and T_e is the effective elastic thickness. We keep the elastic thickness constant within our model simulations as the change in elevation due to erosion and deposition are small relative to the elastic thickness.

2.3 Coupling sediment transport and flexure

Erosion and deposition are coupled to flexure by first solving for the changes in displacement due to an imposed load, p_i (equation 10). The shape of the load is a rectangle 100 km wide and 50 km thick, positioned at the center of the 2000 km long domain, and is described as a density anomaly of between 50 and 100 kgm^{-3}, which forces the lithosphere upwards. In section 3.1 and 3.2 the imposed load is held constant at 50 kgm^{-3}. In section 3.3 we either decrease or increase the magnitude of the load: it is initially100 kgm^{-3} and after 10 Myr of model evolution reduced to 50 kgm^{-3}, or it is initially 50 kgm^{-3} and after 10 Myr of model evolution increased to 100 kgm^{-3}. The initial elevation, z, is given by the displacement due to the imposed load (Figure 2). Topography is of an elevated region flanked by depressions due to the flexural response of the imposed load. These flanking basins are deeper for lower lithosphere elastic thickness (Figure 2, b and c). The load subsequently changes as mass is redistributed by sediment transport (equation 8), where the load due to the sediment transport is $\rho_{fill} g \Delta z$. The elevated central region is eroded and deposition occurs within the flanking basins. For internal sinks within the model, water flows down to the lowest point in both the positive and negative x-directions. It is then assumed that the water leaves the system and the eroded or deposited surface is left behind. The removal of this water could be rationalized as transport of that water out of the plane of the 1-D model.

Sediment transport is solved for using a finite element numerical model. Equations 8 and 9 are made dimensionless where,

$$t = \tilde{t}\frac{L^2}{\kappa} \quad x = \tilde{x}L \quad z = \tilde{z}L \quad q_w = \tilde{q}\alpha L \tag{12}$$

and L is the system length. Equation 8 and 9 become,

$$\partial_{\tilde{t}}\tilde{z} = \partial_{\tilde{x}}\left[\left(1 + D_e\tilde{q}\right)\partial_{\tilde{x}}\tilde{z}\right] \tag{13}$$

and

$$\partial_{\tilde{x}}\left(\frac{\partial_{\tilde{x}}\tilde{z}}{\left|\partial_{\tilde{x}}\tilde{z}\right|}\tilde{q}\right) = -1 \tag{14}$$

where,

$$D_e = \frac{c\alpha L}{\kappa} \tag{15}$$

We use the initial topography or topography from the previous time step, z, to solve equation

14 for the unknown dimensionless water flux, $\tilde{q}$. We solve for the water flux by numerically integrating equation 14. With the water flux calculated then the length dependent diffusion coefficient, $(1+D_e\tilde{q})$, can be calculated for each element within the model domain. Now equation 13 can be solved. The change in topography and displacement is solved implicitly using a finite element method with linear weighting functions. The time step is of 1000 yr on a 1-D grid of 2000 elements.

2.4 Down system grain size distribution

We are interested in looking how change in uplift rate and run-off will alter the stratigraphy in basin successions. We wish to explore the grain size variation in the deposit, yet the sediment flux is assumed to not be a function of grain size. To a first order this assumption is likely reasonable (Paola et al., 1992), although in reality grain size will affect the shear stress required to transport grains down system (e.g. Dade and Friend, 1998). The diffusion coefficient on the Exner equation of mass conservation has been estimated to increase by an order of magnitude once all gravel has been deposited (Marr et al., 2000). However, to maintain the conceptual simplicity of our model, this effect will be ignored.

To explore how stratigraphic grain size may reflect the change in forcing of the system, we use a model of selective deposition by mass (Fedele and Paola, 2007). This model states that greater rates of grain size fining takes place where more deposition occurs. The model solution takes an input grain-size distribution and apportions this input distribution down the basin. For gravel the grain size distribution $\bar{D}$ is given by,

$$\bar{D}(\tilde{x}_d) = \bar{D}_0 + \phi_0 \frac{1}{C_v}\left(e^{-C_g \tilde{y}_d} - 1\right) \qquad (16)$$

where $\tilde{x}_d = x_d / L$ is the dimensionless down-system length of deposition, $\bar{D}_0$ is the mean input grain size, φ_0 is the variance of the input grain distribution C_v=0.25, (Armitage et al., 2011), C_g=0.7 (Duller et al., 2010). $\tilde{y}_d$ is the spatial transformation of $\tilde{x}_d$ given by (Paola and Seal, 1995),

$$\frac{d\tilde{y}_d}{d\tilde{x}_d} = \frac{r(\tilde{x}_d)}{q_s(\tilde{x}_d)} \qquad (17)$$

where $r(\tilde{x}_d)$ is the dimensionless distribution of deposition down system and $q_s(\tilde{x}_d)$ is the equivalent down-system distribution of sediment flux. The model of self-similar grain size fining, equation 16, implicitly assumes that sediment grain size distributions are normal. Therefore the characteristic mean grain size is given by,

$$\bar{D}_0 = \log_{10}\left(D_{50}\right) \quad (18)$$

and the variance is,

$$\phi_0 = \log_{10}\left(\frac{D_{84}}{D_{50}}\right) \quad (19)$$

where D_{50} is the median grain size, D_{84} is the 84 th percentile of the distribution of grain sizes. We chose D_{50} = 40 mm and D_{84} = 70 mm for our model runs.

3 Results

3.1 Model parameters and model evolution in the absence of change

To understand how the basic system behaves, a model with no change in density anomaly (50 kgm^{-3}) and fixed precipitation rates of either 1 or 2 myr^{-1} is presented in Figure 3. We explore the model behavior for two elastic thicknesses, T_e = 20 and T_e = 80 km. Models of erosion and deposition coupled to lithosphere flexure assumed a diffusion coefficient, v, of 100 to 5000 m^2yr^{-1} (Flemings and Jordan, 1989; Sinclair et al., 1991). In our model the diffusivity is also a function of down-system length (Equation 8). To model sediment transport we use the lower value from previous models and assume κ=100 m^2yr^{-1}. For the water flux dependent part, following the derivation of Paola et al. (1992), c in equation 8 can be related to the channel sinuosity, the drag coefficient on the base of the flow, sediment density and sediment concentration in the bed (see equation 7). We will explore the model behavior with c = 0.1 to c= 0.01, which is similar to the values derived by Paola et al. (1992) and Marr et al. (2000). Steady state within this model would manifest in constant values of sediment flux across the system and, for these parameter values, we find that it takes more than 50 Myr for a steady state in sediment flux to be achieved (Figure 3). Furthermore, after 50 Myr of erosion there remains elevated topography at the center of the model domain (Figure 3).

The longevity of the model landscape is not surprising, given that solutions to the sediment transport equation for the erosion of a simple 10 km ramp-like initial condition approach a steady state after 5 Myr in the absence of flexure (Armitage et al., 2013). In Armitage et al. (2013) we showed that for the erosion of a ramp of fixed length with fixed boundary elevation, the time to reach steady state scaled as, $\tau \propto L^2 / \left(\kappa D_e^2\right)$, which from equation 15 can be rewritten as $\tau \propto \kappa / \left(c\alpha\right)^2$. The time scale to reach steady state has a more complex dependence to system length through the solution to a set of simultaneous equations built up of Bessel functions (see Armitage et al., 2013). For example, the timescale associated with a

100 km long landscape is approximately two times longer than for the equivalent 10 km long landscape. However, increasing c, which relates the sediment transport to the surface run-off, by one order of magnitude reduces the response time by approximately two orders of magnitude.

In the coupled models we find that sediment flux decreases substantially during the first 10 Myr for both values of c (Figure 3b, d). If c = 0.01 a 50 % reduction in sediment flux takes 10.5 Myr when the elastic thickness, T_e, is 20 km and 21.9 Myr when T_e is 80 km (Figure 3b). The equivalent reduction in sediment flux for c = 0.1 takes 1.7 and 2.8 Myr respectively (Figure 3d). The long term trend is of a gradual decline in sediment flux after the initial more rapid reduction in sediment flux. When c = 0.01, an 80 % reduction in sediment flux across the model domain takes 50.5 Myr in the case that T_e is 20 km (Figure 3b). If T_e is 80 km an 80 % reduction in sediment flux is not achieved within the 100 Myr model run. For the case where c = 0.1 the equivalent reduction in sediment flux takes 7.2 and 28.6 Myr respectively. Doubling the precipitation rate from 1 to 2 myr^{-1} increases the response time by a factor of two and creates a long-lived increase in sediment flux relative to the model where precipitation rate is 1 myr^{-1} (Figure 3b, d). The characteristic time scale for the denudation of continental landmass is estimated to be on the order of 25 Myr (Pinet and Souriau, 1988). This suggests a lower value of c may be more appropriate. Furthermore, a lower value for c creates topography that has a low concavity, which is appropriate for exploring landscape evolution across continental interiors.

3.2 Signals due to a change in surface run-off

To explore how the idealized system evolves we introduce a smooth transition in precipitation rates after 10 Myr of model evolution (Figure 4a). We explore the response for two elastic thicknesses, T_e = 20 and T_e = 80 km (solid and dashed lines respectively in Figure 4). We also explore the model response for c = 0.1 and 0.01 (see equation 8).

3.2.1 Sediment flux across the model domain

For all model runs there is an increase in sediment flux following an increase in precipitation rates (Figure 4). Sediment flux then slowly reduces, however given the long response time of the coupled model, within the 10 Myr period the system does not recover to the pre-perturbed state (Figure 4b and c). For the case where c = 0.01, the magnitude of the sediment flux response is larger than if c = 0.1 (Figure 4b and c). This is because when c = 0.1 the landscape has lower gradients due to the effectiveness of sediment transport at removing mass (Figure 3c). A reduction in precipitation rates leads to a reduction in sediment flux, with the system

similarly shifting to a new prolonged state of gradually reducing sediment flux (Figure 4d and e). Again when c is larger the magnitude of the response is lower due to the overall reduction in slope following increased erosion.

The long lived state of increased/decreased sediment flux described above is caused by the interplay between the change in topography driven by the mantle density anomaly, and by the change in load due to erosion and deposition. As precipitation rate is changed, erosion and flanking deposition change. This re-distribution of mass continuously modifies the distribution of rock uplift and acts to maintain similar gradients across the 1-D landscape. The result is that sediment flux remains at an elevated value for long periods of time (Figure 5).

The change in precipitation rate is being imposed before the system has achieved a steady state. The coupled model takes more than 50 Myr to achieve a significant reduction in sediment flux (Figure 3). In previous models of erosion driven by similar transport laws, but where uplift is imposed as a vertical velocity rather than an instantaneous adjustment to a buoyant load upon an isostatic compensated lithosphere, a single step increase in precipitation rate generated a spike in sediment flux that recovered to the same steady state sediment flux prior to the change (Armitage et al., 2011). Increasing precipitation for that same model but before the model had recovered to steady state, resulted in a reduced signal in terms of sediment flux out of the catchment that nonetheless recovered to the same steady state signal of sediment flux out of the catchment (Armitage et al., 2013). In the model we present in this paper, increasing precipitation leads to a long recovery time and even after 20 Myr the sediment flux signal will not attain similar values for different precipitation rates (Figure 3). Such a long recovery of sediment flux is not predicted by these previous models (Armitage et al., 2011; Armitage et al., 2013).

3.2.2 Stratigraphy

Throughout the full 20 Myr period for all models there is a general trend of progradation (Figure 6 and 7). This progradation is a function of the system slowly evolving towards a steady output of sediment flux (Figure 3 and 4). The response recorded within stratigraphy of an increase in precipitation rate is difficult to observe without a close inspection of Figure 6 or 7.

For the case where $c = 0.01$, upon the increase in precipitation rates there is a thickening over time of depositional units and a gradual increase in depositional length above the background rate at 10 Myr, associated with the increase in sediment delivery (Figure 6b, c and g, h). The lack of a strong signal of stratigraphic progradation, such as that predicted within the model of

Armitage et al. (2011), is because accommodation keeps pace with sediment supply. This is because, within the coupled model, the flexural response is a combination of: (1) the load of the sediment, (2) the erosion and (3) the imposed density anomaly, which work together to increase accommodation space generation such that there is no significant change in the rate of grain size fining. The stratigraphic response to a reduction in precipitation rates is a thinning of the stratigraphic units, but likewise there is no strong response within the granulometry, other than a minor reduction in the rate of progradation at 10 Myr (Figure 6a, b and d, e).

For the case where $c = 0.1$ there is an increase in transport of sediment due to the flow of water, q_w. This causes increased erosion and deposition such that the landscape becomes quite flat within 20 Myr (maximum slope of 2.6×10^{-4} at 20 Myr; Figure 3c and 7). We have plotted the stratigraphic record for an elastic thickness of 20 km only in Figure 7, as for a 80 km elastic thickness, the resulting record shows the same trend but with thinner deposits. The stratigraphic evidence for change in precipitation rate is migration of the erosion-deposition transition (Figure 7). Otherwise there is little evidence within the stratigraphy of the change in precipitation.

For all of the models at young ages sediment is deposited outside of the main basin due to wider flexural bulges that are shallow. These wider deposits are very thin and are eventually buried beneath the main basins. Sediment is also transported into the basins from both directions, leading to a deposit of coarser material along the far edge of the main basin. This deposition is analogous to that expected within the hanging wall of a fault controlled basin.

3.3 Signals due to change in upper mantle buoyancy

We introduce an increase or decrease in topography by changing the magnitude of the density anomaly in the upper lithosphere (Figure 8a), which causes tilting of the landscape. Again we model two elastic thickness and two values of c (see equations 8 and 10).

3.3.1 Sediment flux across the model domain

Increasing the magnitude of the density anomaly that maintains the elevated central region in the model domain from 50 to 100 kgm^{-3}, for both values of c (0.01 and 0.1), causes sediment flux to initially increase and then decrease as the system re-equilibrates (Figure 8b and c). This behavior is similar to that predicted for an increase in run-off, where after the initial perturbation, the interplay between load and topography causes a gradual reduction in sediment flux as the system evolves. The key difference between a change in density anomaly and run-off is that slopes change significantly when the density anomaly is changed (Figure

9).

For the case where $c = 0.01$ the response to a reduction in buoyancy in the upper mantle is a reduction in sediment flux (Figure 8d). When the elastic thickness is 20 km there is an additional short lived (~1 Myr) relative drop in sediment flux (Figure 8d, solid line). This minimum is due to a transient period where the imposed reduction in density driving topographic change creates a platform like elevated region, or plateau, in the center of the model domain (Figure 10a, 11 Myr). Sediment flux increases briefly as the edges of this plateau are eroded at between 10 and 11 Myr. The model then evolves towards a landscape with a central peak of reduced elevation after 20 Myr (Figure 10a).

For the case where $c = 0.1$ a reduction in buoyancy creates an increase in sediment flux off the eroding regions within the model domain (Figure 8e). This is because when the effect of water flux on sediment transport is larger, the reduction in the density anomaly from 100 to 50 kgm^{-3} creates a central depression (Figure 10b). As topography lowers due to the reduced magnitude of the density anomaly, the flexural bulge due to the flanking basins becomes responsible for the generation of the greatest elevation at a model distance of 750 and 1250 km (Figure 10b, 11 Myr). The whole structure then inverts, as central deposition and flanking erosion act to lower topography until the landscape is almost flat (maximum slope of 1.7×10^{-4} at 20 Myr; Figure 10b). This inversion of topography is responsible for the increase in sediment flux when the density anomaly is reduced (Figure 8e).

3.3.2 Stratigraphy

The stratigraphic response to a change in topography due to the mantle density anomaly is quite different from that of a change in run-off. For an increase in relief due to an increase in the buoyancy a retrogradation of the depositional system and of grain size is recorded (Figure 11b, c, g, h and Figure 12b, c, g, h). This phase of retrogradation and increase in grain size fining is transient however, resulting from a temporary reduction in sediment supply relative to accommodation space. Accommodation space increases due to the flexure of the lithosphere as a consequence of increased upper mantle buoyancy. As can be seen within the chronostratigraphic diagram (Figure 11 and 12) the depositional front has an up-system trajectory at 10 Myr, and then deposition gradually migrates back down-system with an associated lengthening of the depositional system. This signal is stronger when $c = 0.1$ (Figure 12).

A reduction in the density anomaly that provides the buoyancy driven support of the landscape creates a very different response, which is strongly dependent on the strength of

sediment transport as a function of water flow (Figure 11a, b, e, f, and Figure 12a, b, e, f). For the case where $c = 0.01$ a reduction in buoyancy causes the depositional system to prograde (Figure 11a, b, e, f). This progradation is a consequence of a reduction in elevation which causes a forward migration of the depositional front. This pushes the coarse deposits forwards. In the case of a 20 km elastic thickness, a short-duration (~ 1 Myr) coarse unit is deposited upon the central elevated region and subsequently eroded away (Figure 11e, f).

If the effect of run-off is stronger, $c = 0.1$, then there is inversion, which is to say that the centrally elevated region becomes a depo center (Figure 12a, b, e, f). This is due to the density anomaly being of too small a magnitude to maintain the central elevation. Instead the flanking deposits create the highest elevation due to flexure of the lithosphere at a distance of roughly 750 and 1250 km (Figure 10b and 12a, e). Deposition then switches into the central basin and the flanking basins become abandoned (Figure 12a, b, e, f).

4 Discussion

We have presented a model for the transport of sediment to calculate the change in topography across a 2000 km region for a change in relief driven by change in density within a 100 km wide 50 km thick region in the upper mantle. Parameter values for the model of sediment transport are justifiable based on up-scaling empirical bed-load transport laws and are similar to previous models of that couple deposition and lithosphere flexure (e.g. Flemings and Jordan, 1989; Sinclair et al., 1991; Paola et al., 1992). These parameter values lead to a topography that has a low concavity and hence a low relief, which is appropriate for exploring processes in the continental interior away from large mountain belts. The spatially changing load due to erosion and deposition alters topography as the modeled purely elastic lithosphere adjusts isostatically. This model suggests the following:

(1) In our model the amount of material transported by the flow of water is controlled by the parameter c (equation 8). The value of c can be estimated from the basic properties of alluvial sediment transport and is roughly between 1 and 0.01 (Paola et al., 1992; Marr et al., 2000). We have explored the lower end of this range and found that for $c = 0.1$ to 0.01 the response time is between 1 and 20 Myr (Figure 3). For $c = 0.1$ landscape becomes relatively flat after 20 Myr and the magnitude of change in sediment flux, following a change in precipitation or buoyancy in the upper mantle is small (Figures 4, 8 and 10). If the we increase c to 1, as suggested for sand transport (Marr et al., 2000), then topography that is generated by buoyancy within the upper mantle would be eroded down over a shorter period of time, < 1 Myr, as the response time is inversely proportional to c, $\tau \propto \kappa / (c\alpha)^2$ (see Section 3.1).

In the case where the transport of sediment due to water flow is weak, $c = 0.01$, then the time scale of response to change is close to that estimated for continental denudation, 25 Myr (Pinet and Souriau, 1988). It is likely that c is not a fixed value in space or time as sediment gets moved and the distribution of gravel and sand changes, however our modeling study suggests that on a gross scale if $c > 0.1$ landscape may be effectively beveled off, while if $c < 0.1$ elevated regions will remain elevated for more than 100 Myr (Figure 3). Therefore, for modeling long term sediment transport, we suggest that $c \sim 0.01$ is more reasonable.

(2) A change in run-off due to an increase or decrease in precipitation rate causes an increase or decrease in sediment flux out of the region of erosion (Figure 4). The change in erosion and deposition affects the surface load, which facilitates isostatic uplift that keeps pace with the denudation. The result is that a change in run-off causes only a minor change in catchment slope (Figure 5). The depositional system thickens and gradually lengthens as the system evolves, and consequently, grain size fining does not vary significantly (Figure 6 and 7).

(3) An increase in relief driven by an increase in upper mantle buoyancy causes an increase in sediment flux (Figure 8b and c). This increase in sediment flux is accompanied by a transient phase of retrogradation of the depositional system, shown as a vertical reduction in grain size (Figure 11c, d, g, h and 12c, d, g, h). The transient retrogradation phase is due to the increase in the rate of accommodation space generation relative to sediment flux. Accommodation space is generated in the model by the flexural bulge that flanks the uplifted central region (Figure 2 and 3). The instantaneous flexural response means that for greater contrast in density, the elevation of the central region of the model and the amount of subsidence in the flanking basins becomes greater. This increases the accommodation space for sediment at a pace that is more rapid compared to the rate of increase in sediment delivery to the basin.

(4) A reduction in the buoyancy that maintains the elevated central region causes marked progradation of the depositional front if the transport of sediment due to run-off is low, $c = 0.01$ in equation 8 (Figure 11a, b, e, f). Progradation is due to the drop in topography creating a reduction in slope so that the region of positive curvature migrates outwards. Elevated topography is due to the imposed buoyancy and also due to the flexural response of the flanking load. The combination of the buoyancy and flexure causes the central elevated region to widen as deposition migrates outwards. If sediment transport due to water flow is high, $c = 0.1$, then the reduced buoyancy cannot maintain the central high and the system inverts, creating a central basin where there was previously an elevated region (Figure 10b, 12a, b, e, f). The flexural response to the flanking basins creates two elevated regions either side of a central depo center. This central basin then starts to fill as the topography flattens.

These numerical experiments demonstrate that the stratigraphic signature of change in tilt of the continental interior due to mantle flow is delicately controlled by the strength of erosion and deposition due to sediment transport, and mediated by the lithospheric response.

4.1 Comparison with previous transport-limited models

Earlier models that use a similar approach for sediment transport but with a different mechanism for creating change in topography have predicted both similar and different potential records of sediment accumulation. The response of this model to a change in relief due to a change in the density anomaly that drives topographic change has similarities to the previous short normal fault controlled sedimentary fan development models of Paola et al. (1992), Densmore et al. (2007), and Armitage et al. (2011). This similarity is due to the change in fining being due to a similar shift in the ratio of sediment supply to accommodation: in section 3.3, an increase in catchment elevation driven by increased buoyancy, accommodation space increases faster than supply. The predicted signals left in the stratigraphic record due to a change in run-off are however different. In the normal fault bounded mountain catchment-fan model of Armitage et al. (2011), an increase in run-off is predicted to generate prograding conglomeratic sheet-like deposits with sediment fluxes reducing to steady-state values after a million years. However, in section 3.2, we found that for large systems, where topography change is by a flexural response to change in load from both the upper mantle and surface, a change in run-off generates only a minor signal within the granulometry accompanied by a prolonged (> 10 Myr) increase in sediment fluxes.

There are three key differences between the model developed here and the previous models of fault bound catchment-fans that reduce the impact of change in precipitation on the sedimentary record:

(1) Response times are very long in this coupled model (Figure 3). The increased response time is due in part to the choice of parameters (κ and c in Equation 8). The values of these parameters are based on reasonable estimates of basic physical properties of bed-load transport and are similar to previous numerical models. It is clear that increasing c or decreasing κ will decrease the initial model response time to change in precipitation. However, the long term gradual decline in sediment flux out of the central elevated region is a function of the interplay between unloading and loading due to sediment transport. This keeps slopes elevated and allows the continued transport of material above an equilibrium value for at least 50 Myr (Figure 3).

(2) A change in precipitation does not cause a significant change in slope (Figure 5).

Increasing precipitation rates, for example, increases the load at the flanking basins and reduces the load in the central high. The instantaneous flexural response causes the eroded area to rise and the deposited regions to sink. This feedback between the removal of mass and the rebound of the surface topography keeps slopes roughly similar as precipitation is increased. Therefore, sediment flux increases and does not reduce rapidly as is the case for models where flexure of the lithosphere and isostasy were ignored (e.g. Armitage et al., 2011).

(3) Accommodation space is not fixed or controlled by tectonic faulting. This allows the basin to decrease and increase in size as the sediment loading increases. The result is that if sediment delivery to the basin is increased then the accommodation space will likewise increase. Thus a change in precipitation has very little impact on the stratigraphic record in terms of vertical granulometry (Figure 6 and 7).

Within the construct of our model, the deposition of coarser grains in the form of a temporarily uniform far – traveled conglomeratic sheet only occurs upon a reduction in the mantle density anomaly driving tilt of the surface (Figure 11). Such behavior is similar to that proposed by Heller et al. (1988). In Heller et al. (1988) it is suggested that widespread/far-travelled conglomerate units are deposited as mountain building ends. This hypothesis was immediately questioned based on depositional ages within the northwest Himalaya (Burbank et al., 1988), where coarser deposits prograde further down-system with time and is related to rejuvenated uplift within the axial zone of the Himalaya. What we find is that an increase in elevation due to upper mantle buoyancy does produce a down-system migration of larger grain sizes, but this gradual progradation is a symptom of the system evolving towards a steady state, rather than a direct signal of an increase in topography within the eroding landscape. We propose that coarse and laterally extensive gravel deposits are most likely a result of a reduction in catchment uplift and basin subsidence, or a reduction in tilt.

4.2 Late Cenozoic erosion and deposition in southwestern North America

During the latest Cretaceous to Paleocene a number of far-traveled conglomerate units that were formed in southeastern North America. These deposits lie above a disconformity and travel down the length of the basin (Heller et al., 2013). Subsidence analysis of the basins that contain these deposits would locate deposition occurring after a period of subsidence increase (see Heller et al., 2013, their Figure 4). In other words, deposition of gravel units occurs once subsidence reduces. In the more recent geological past there is evidence for two periods of change in denudation within southwestern USA during the late Cenozoic, which might be related to the deposition of far-traveled conglomeratic units and could be a function of change

595 in climatic conditions or due to long-wavelength tilting due to mantle flow:

(1) During the Late Oligocene to Early Miocene (27 to 15 Ma) there is widespread erosion and fluvial incision ranging from the Colorado Plateau, the southern Great Plains and central and western Texas (Chapin, 2008; Flowers et al., 2008; Cather et al., 2012). This period of denudation was synchronous with extension and foot-wall uplift within the Basin and Range
600 and Rio Grande Rift, and ends with the widespread deposition of coarse grain units, the Ogallala, Bidahochi and Fence Lake Formations (Cather et al., 2012). The Late Oligocene to Early Miocene also corresponds with a period of significant change in ocean circulation, with the closure of the Tethys Ocean between Europe and Africa, and increased deep water formation through the Faroes-Scotland Ridge (see review by Chapin, 2008).

605 (2) During the Late Miocene to Pliocene (6 to 3 Ma) there is clear incision of the Ogallala deposits and evidence of tilting of the pre-incised surface (McMillan et al., 2002; Duller et al., 2012). The incision of the Ogallala deposits may have been driven by increased surface run-off (Wobus et al., 2010), and the tilt is subsequently a consequence of that erosion as the lithosphere isostatically compensates for the change in surface load. However, it could be that
610 the tilt is due to change in the density structure of the mantle and crust, associated with warmer mantle and ignimbrite eruptions along the Jemez lineament (Wisniewski and Pazzaglia, 2002; Nereson et al., 2013), and the period of uplift lead to incision of the Ogallala deposits.

We will apply our model to the Ogallala Formation, to explore if the change in depositional
615 slope and change in gravel units deposited are more likely due to change in run-off or tilting of the continental interior. The Ogallala Formation can be split into four units of between 50 and 100 m thickness and 250 to 300 km length each of duration of 4 Myr. Assuming each unit has a cross-sectional area in the shape of a triangle, the sediment flux required to deposit the Ogallala is between 1.5 and 3.8 m^2yr^{-1}. This magnitude of sediment flux is consistent with
620 that generated by our model of sediment transport where $c = 0.01$ (Figure 3b and d).

The Late Cenozoic Ogallala Formation is perhaps thicker than the earlier Cretaceous - Paleocene deposits that is associated with a reduction in subsidence (Heller et al., 2013). Yet it is plausible that their deposition marks the tail end of regional uplift within the Rio Grande Rift zone and the Colorado Plateau. The Ogallala deposits (18 to 6 Ma; Swinehart et al.,
625 1985) are potentially correlated with volcanism and northward propagation of the Rio Grande Rift zone (e.g. McMillan et al., 2002). However, their deposition post-dates peak volcanism within Colorado and New Mexico (~ 35 Ma; McMillan et al., 2000) and the onset of extension within the Rio Grande itself (Chapin and Cather, 1994). Recent apatite (U-Th)/He

data would suggest that extension within the northern and southern Rio Grande Rift was coeval, and there was no northward propagation of the rift zone (Landman and Flowers, 2013). It is therefore possible that regional uplift decreased after ~15 Myr, after the main phase of extension, which is supported by thermochronometric measurements that suggest the Colorado Plateau has experienced little or no change in elevation since this time (Huntington et al., 2010). Therefore, as uplift reduced, the depositional system migrated down-stream causing incision of the upper deposits and the progradation of coarse units onto the Great Plains.

In the last ten million years there has been further change in the topography of the southwest USA (Figure 13a, b). Observations would suggest that the Ogallala deposition surface was tilted at or before 6 Ma as the present day slope of the Ogallala is steeper than the reconstructed transport slope of the Ogallala (Leonard, 2002; McMillan et al., 2002; Duller et al., 2012; Figure 13a). From outcrop patterns of the Ogallala and Remsburg Ranch units we can infer that the flexural hinge is located ca. 160-200 km east of the Wyoming-Nebraska Border (Swinehart and Diffendal 1995, 1997; Duller et al., 2012). The transport slope of the Ogallala during the formation of this layer is similar to the present day slope of the North Platte River (Duller et al., 2012; Figure 13a). This phase of uplift may be associated with increased temperatures in the mantle that lead to uplift of the surface, and rejuvenated volcanism within the Jemez lineament (Nereson et al., 2013). This uplift may also be related to the Aspen seismic anomaly to the south (Karlstrom et al., 2012). This 100 to 300 km wide anomalous low seismic velocity zone within the upper mantle is associated with a low Bougier gravity anomaly, which would suggest a buoyant crust and upper mantle supports the high topography. Karstrom et al. (2012) propose from thermochronologic and geologic data that regional exhumation accelerated starting ca. 6–10 Ma, particularly within regions like that above the Aspen low-velocity zone. This would suggest that Neogene mantle convection has driven long-wavelength surface deformation and tilting over the past 10 Ma (Karlstrom et al. 2012).

It is estimated that the surface underwent up to 600 m of increased elevation to the west (Leonard, 2002; McMillan et al., 2002; Duller et al., 2012), and the surface was then incised prior to deposition of the Broadwater Formation (Duller et al., 2012). If we assume that the lithosphere has an elastic thickness of 80 km, which gives a flexural rigidity of 4.55×10^{24} Nm and is comparable with estimates of Leonard (2002) and that $c = 0.01$ to be consistent with estimated sediment flux, then a decrease in buoyant support of topography by reducing the density anomaly from 100 to 50 kgm^{-3} generates a slope change of roughly 4×10^{-3} within 3 Myr of model evolution (Figure 13c). Such a change in slope is comparable to that estimated

to have had occurred between 6 and 3.7 Ma (Duller et al., 2012). The model suggests that a significant change in slope due to an increase in surface run-off is however not possible (Figure 5).

Based on our idealized model of sediment transport coupled to an isostatically compensated lithosphere, we propose that the observed Late Cenozoic pattern of deposition within the Great Plains is primarily driven by change in catchment uplift as the Eastern Rocky Mountains are gently tilted by density changes within the mantle. Over the last 30 Ma two pulses of transient uplift have left behind the Ogallala Formation and its subsequent incision. The counter hypothesis, that this history in deposition is a consequence of change in run-off is not consistent with our model of sediment transport coupled to lithosphere flexure.

5 Conclusions

We have developed a model of sediment transport coupled to an isostatically compensated lithosphere. It is contentious to suggest that the whole of the continental interior is covered in transportable regolith, however given that sediment covers large proportions of the USA (Millar and White, 1998), we suggest that this transport-limited model is appropriate for modeling gross change in deposition across the continental interior. Based on this model we propose the following:

(1) In the absence of tectonically controlled basin formation, change in run-off does not have a strong signature in the stratigraphic record.

(2) Change in topography due to change in uplift rates causes signals of progradation or retrogradation for a reduction or increase in uplift.

When we apply these model results to the history of the southwestern USA we propose that the deposition of gravel conglomerate deposits that span millions of years, such as the Ogallala Formation, are due to a drop in catchment uplift and basin subsidence. For the case of the Ogallala, this drop in catchment elevation is likely due to the ending of the Cenozoic (27 to 15 Ma) period of extension in the Rio Grande Rift zone. Uplift within the Eastern Rocky Mountains reduced at roughly 15 Ma and consequently deposition migrated outwards onto the Great Plains and southwards creating the Ogallala Formation.

More recent (>6 Ma) uplift and incision of the Ogallala is more likely due to a recent phase of uplift of the Great Plains associated with change in density within the upper mantle. There is strong evidence for buoyancy within the upper mantle below regions such as Aspen, Colorado, which is a likely source of such buoyancy driven support of high topography. Such a change in topography due to mantle buoyancy is more likely to have promoted incision of

previous deposits, as our model would suggest that erosion due to increased run-off has little effect on topography and transport slope.

Acknowledgments

This work was funded by a Marie Curie research fellowship (project number 272669) and has continued support through a Royal Astronomical Society Research Fellowship to John Armitage. The authors would like to thank Peter Burgess and Philip Allen for their comments on this manuscript. The authors would also like to thank Chris Paola, Greg Tucker and the editor Eric Kirby for very constructive and thorough reviews.

Figure Captions

Figure 1: Diagram showing the conservation of mass within a 2-D domain, where mass enters the system through uplift, U (units of myr^{-1}), and exists as sediment transported, q_s (m^{2}yr^{-1}) out of the domain. P (myr^{-1}) is the rate of production of regolith, h (m), is the thickness of regolith, η (m), is the bedrock elevation and, z (m), is the total elevation.

Figure 2: Diagram of model domain and initial topography. (a) Cartoon of lithosphere asthnosphere system where a permanent negative buoyant load drives the surface upwards to create an elevated central region. (b) Initial topography when the elastic thickness is 20 km. (c) Initial topography when the elastic thickness is 80 km.

Figure 3: Model evolution for a constant buoyancy in the upper mantle. (a) Topography at 0.1, 50 and 100 Myr of model evolution for the case where c in equation 8 is 0.01 and the elastic thickness is 20 k. This case has a weaker dependence on water flux. (b) Flux of sediment eroded off half of the symmetric model domain, 0 to 1000 km distance, for three models: two where c = 0.01 and precipitation is 1 myr^{-1}. These two models have different elastic thickness of 20 and 80 km (solid and dashed lines). (c) and (d) are the equivalent model evolution where dependence on water flux is stronger, c = 0.1 in equation 8. In part c the topography is plotted for 0.1, 10 and 50 Myr because after 50 Myr the landscape is almost flat.

Figure 4: Model response to a change in precipitation rate after 10 Myr. (a) curves for the imposed change in precipitation rate, where the change is prescribed to be smooth. (b) Sediment flux off half of the eroding model domain, 0 to 1000 km distance (Figure 3) as the

model is symmetric. Two models are presented for an increase in precipitation rate from 0.5 to 1 myr^{-1} where c = 0.01 (see equation 8). The solid line is for an elastic thickness of 20 km and the dashed line is for 80 km. (c) Sediment flux for the same increase in precipitation rate when c = 0.1 (see equation 8). (d) Sediment flux for a decrease in precipitation rates from 1 to 0.5 myr^{-1} where c = 0.01 and (e) when c = 0.1.

Figure 5: Maximum slope for a change in precipitation for the model where c= 0.01 and the elastic thickness is 20 km. The change in slope for an increase in precipitation is the dashed line and a decrease is the solid line. The change in precipitation occurs at 10 Myr.

Figure 6: Stratigraphy at 2 Myr intervals and granulometry as the model responds to a change in precipitation rate where the dependence of sediment transport on water flow is weak, c = 0.01 in equation 8. (a) top to bottom Response to a precipitation decrease from 1 to 0.5 myr^{-1} at 10 Myr (see Figure 4) assuming the elastic thickness is 80 km. (b) Chronostratigraphic diagram for the same conditions as part a. (c) Response to a precipitation increase from 0.5 to 1 myr^{-1} assuming the elastic thickness is 80 km. (d) Chronostratigraphic diagram for the same conditions as part c. (e) Response to a precipitation decrease assuming the elastic thickness is 20 km. (f) Chronostratigraphic diagram for the same conditions as part e. (g) Response to a precipitation increase assuming the elastic thickness is 20 km. (h) Chronostratigraphic diagram for the same conditions as part g. During the early evolution there is a downward fining from both the left and right hand sides of the basins due to sediment delivery from both sides of the basin.

Figure 7: Stratigraphy at 2 Myr intervals and granulometry as the model responds to a change in precipitation where the dependence of sediment transport is strong, c = 0.1 in equation 8. (a) Response to a precipitation increase from 0.5 to 1 myr^{-1} at 10 Myr (see Figure 4). (b) Chronostratigraphic diagram for the same conditions as part a. (c) response to a decrease in precipitation from 1 to 0.5 myr-1 at 10 Myr, and (d) the equivalent chronstratigraphic diagram. Elastic thickness is 20 km throughout this figure. During the early evolution there is a downward fining from both the left and right hand sides of the basins due to sediment delivery from both sides of the basin.

Figure 8: Model response to a change in density after 10 Myr that drives the buoyancy and

keeps the central part of the model domain elevated. (a) curves for the imposed change in density, where the change is prescribed to be smooth. (b) Sediment flux off half of the eroding model domain, 0 to 1000 km distance (Figure 3) as the model is symmetric. Two models are presented for an increase in density anomaly from 50 to 100 kgm^{-3} where $c = 0.01$ (see equation 8). The solid line is for an elastic thickness of 20 km and the dashed line is for 80 km. (c) Sediment flux for the same increase in density anomaly when $c = 0.1$ (see equation 8). (d) Sediment flux for a decrease in density anomaly from 100 to 50 kgm^{-3} where $c = 0.01$ and (e) when $c = 0.1$.

Figure 9: Maximum slope for change in the density anomaly driving surface tilt. The solid line is for a decrease in density anomaly for the case where $c = 0.01$ and the elastic thickness is 20 km. The dashed line is the equivalent model where the buoyancy is increased.

Figure 10: Topographic evolution for a reduction in the density difference that generates the central elevated region within the model domain. (a) Change in topography as density is reduced (Figure 8a) when the dependence of sediment transport on water flow is weak, $c = 0.01$. The topography transitions from a central elevation of 800 m to a elevation of 200 m by temporarily taking the form of a plateau like structure. (b) Change in topography as density is reduced when the dependence of sediment transport on water flow is strong, $c = 0.1$. In this case at 11 Myr the elevated regions are a consequence of the flexural response due to the flanking deposits, creating a central low in which sediments accumulate.

Figure 11: Stratigraphy at 2 Myr intervals and granulometry as the model responds to a change in the density of the mantle anomaly driving surface tilt where the dependence of sediment transport on water flow is weak, $c = 0.01$ in equation 8. (a) top to bottom Response to a load decrease from 100 to 50 kgm^{-3} assuming the elastic thickness is 80 km. (b) Chronostratigraphic diagram for the same conditions as part a. (c) Response to a load increase from 50 to 100 kgm^{-3} assuming the elastic thickness is 80 km. (d) Chronostratigraphic diagram for the same conditions as part c. (e) Response to a load decrease assuming the elastic thickness is 20 km. (f) Chronostratigraphic diagram for the same conditions as part e. (g) Response to a load increase assuming the elastic thickness is 20 km. (h) Chronostratigraphic diagram for the same conditions as part g. During the early evolution there is a downward fining from both the left and right hand sides of the basins due to sediment delivery from both sides of the basin.

Figure 12: Stratigraphy at 2 Myr intervals and granulometry as the model responds to a change in the density of the mantle anomaly driving surface tilt where the dependence of sediment transport on water flow is strong, $c = 0.1$ in equation 8. (a) top to bottom Response to a load decrease from 100 to 50 kgm^{-3} assuming the elastic thickness is 80 km. (b) Chronostratigraphic diagram for the same conditions as part a. (c) Response to a load increase from 50 to 100 kgm^{-3} assuming the elastic thickness is 80 km. (d) Chronostratigraphic diagram for the same conditions as part c. (e) Response to a load decrease assuming the elastic thickness is 20 km. (f) Chronostratigraphic diagram for the same conditions as part e. (g) Response to a load increase assuming the elastic thickness is 20 km. (h) Chronostratigraphic diagram for the same conditions as part g. During the early evolution there is a downward fining from both the left and right hand sides of the basins due to sediment delivery from both sides of the basin.

Figure 13: Present-day and reconstructed slopes for the Ogallala and Broadwater Formation from 10 Ma to present and a comparison to model slope due to a reduction in mantle-driven uplift rate. (a) Present-day and reconstructed slopes of the Ogallala, Broadwater Formations and the modern North Platte River (see Duller et al., 2012). The Ogallala Formation was deposited with transport slopes similar to the modern day, and was subsequently tilted up to the west. (b) Simplified fluvial successions of the Nebraskan Great Plains post 10 Ma, showing the Ash Hollow Formation within the tail end of the Ogallala Formation, and the 3.7 Ma Broadwater Formation. (c) Model topography plotted across the transition in erosion to deposition for a 50 kgm-3 reduction in density anomaly driving uplift, see Figures 3c, d and 7a,b. Topography is plotted at 10 Myr and 13 Myr, which spans the period of uplift rate reduction. The change in topography for this forward model is similar to the observed change in slope between the Ogallala and Broadwater Formations.

Table Caption

Table 1: Model parameters and assumed values.

References

Armitage, J. J., Duller, R. A., Whittaker, A. C., Allen, P. A., 2011. Transformation of tectonic and climatic signals from source to sedimentary archive. Nature Geoscience 4, 231–235, doi:10.1038/ngeo1087.

Armitage, J. J., Dunkley Jones, T., Duller, R. A., Whittaker, A. C., Allen, P. A., 2013. Temporal buffering of climate-driven sediment flux cycles by transient catchment response. Earth and Planetary Science Letters 369-370, 200–210, doi: 10.1016/j.epsl.2013.03.020.

Blum, M.D. and Tornqvist, T.E., 2000. Fluvial responses to climate and sea-level change: a review and look forward. Sedimentology, 47, 2-48, suppl. 1

Boettcher, S. S., Milliken, K. L., 1994. Mesozoic-Cenozoic unroofing of the Southern Appalachian Basin: apatite fission track evidence from Middle Pennsylvanian sandstones. Journal of Geology 102, 655–686.

Burbank, D. W., Beck, R. A., Raynolds, R. G. H., Hobbs, R., Tahirkheli, R. A. K., 1988. Thrusting and gravel progradation in foreland basins: a test of post-thrusting gravel dispersal. Geology 16, 1143–1146.

Burgess, P. M., Gurnis, M., 1995. Mechanisms for the formation of cratonic stratigraphic sequences. Earth and Planetary Science Letters 136, 647–663.

Castelltort, S. and van der Driessche, J., 2003. How plausible are high-frequency sediment supply-driven cycles in the stratigraphic record? Sedimentary Geology, 157, 3-13, doi: 10.1016/S0037-0738(03)00066-6

Cather, S. M., Chapin, C. E., Kelly, S. A., 2012. Diachronous episodes of Cenozoic erosion in southwestern North America and their relationship to surface uplift, paleoclimate, paleodrainage and paleoaltimatry. Geosphere 8, 1177–1206, doi: 10.1130/GES00801.1.

Chapin, C. E., 2008. Interplay of oceanographic and paleoclimate events with tectonism during middle to late Miocene sedimentation across the southwestern USA. Geosphere 4, 976–991, doi: 10.1130/GES00171.1.

Chapin, C. E., Cather, S. M., 1994. Tectonic setting of the axial basins of the northern and central Rio Grande Rift. In: Keller, G. R., Cather, S. M. (Eds.), Basins of the Rio Grande Rift: structure, stratigraphy and tectonic setting. Geological Society of America Special Paper 291. Geological Society of America, pp. 5–25.

Coakley, B., Gurnis, M., 1995. Far-field tilting of Laurentia during the Ordovician and constraints ont eh evolution of a slab under an ancient continent. Journal of Geophysical Research 100 (B4), 6313–6327.

Dade, W. B., and Friend, P. F., 1998. Grain size, sediment transport regime, and channel slope in alluvial rivers. The Journal of Geology, 106, 661-676.

Densmore, A. L., Allen, P. A., Simpson, G., 2007. Development and response of a coupled

catchment fan system under changing tectonic and climatic forcing. Journal of Geophysical Research 112 (F01002), doi: 10.1029/2006JF000474.

Dietrich, W. E., Bellugi, D. G., Sklar, L. S., Srock, J. D., Heimsath, A. M., Roering, J. J., 2003. Geomorphic transport laws for predicting landscape form and dynamics. In: Wilcock, P. R., Iverson, R. M. (Eds.), Prediction in Geomorphology. Vol. 135 of Geophysical Monograph. American Geophysical Union, pp. 1–30, doi: 10.1029/135GM09.

Duller, R. A., Whittaker, A. C., Fedele, J. J., Whitchurch, A. L., Springett, J., Smithells, R., Fordyce, S., Allen, P. A., 2010. From grain size to tectonics. Journal of Geophysical Research 115 (F03022), doi: 10.1029/2009JF001495.

Duller, R. A., Whittaker, A. C., Swinehart, J. B., Armitage, J. J., Sinclair, H. D., Bair, A., Allen, P. A., 2012. Abrupt landscape change post-6 Ma on the central Great Plains, USA. Geology 40, 871–874, doi: 10.1130/G32919.1.

Exner, F. M., 1920, Zur Physik der Dunen, Sitzber. Akad. Wiss Wien, Part IIa, Bd. 129.

Fedele, J. J., Paola, C., 2007. Similarity solutions for alluvial sediment fining by selective deposition. Journal of Geophysical Research 112 (F02038), doi: 10.1029/2005JF000409.

Flemings, P. B., Jordan, T. E., 1989. A synthetic stratigraphic model of foreland basin development. Journal of Geophysical Research 94 (B4), 3851–3866, doi: 10.1029/JB094iB04p03851.

Flemings, P. B., Jordan, T. E., 1990. Stratigraphic modeling of foreland basins: Interpreting thrust deformation and lithosphere rheology. Geology 18, 430–434.

Flowers, R. M., Wernicke, B. P., Farley, K. A., 2008. Unroofing, incision and uplift history of southwestern Colorado Plateau apatite (U-Th)/He thermochronometry. Geological Society American Bulletin 120, 571–587, doi: 10.1130/B26231.1.

Gallen, S. F., Wegmann, K. W. and Bohnenstiehl, D. R., 2013. Miocene rejuvenation of topographic relief in the southern Appalachians. GSA Today, 23, 4-10, doi: 10.1130/GSATG163A.1.

Granjeon, D., Joseph, P., 1999. Concepts and applications of a 3-D multiple lithology, diffusive model in stratigraphic modelling. In: Harbaugh, J. W., Watney, W. L., Rankey, E. C., Slingerland, R., Goldstein, R. H. (Eds.), Numerical Experiments in Stratigraphy. Vol. 62 of Special Publications. Society for Sedimentary Geology, pp. 197–210, doi: 10.2110/pec.99.62.0197.

Heller, P. L., Angevine, C. L., Winslow, N. S., Paola, C., 1988. Two-phase stratigraphic

model of foreland-basin sequences. Geology 16, 501–504.

Heller, P. L., Mathers, G., Dueker, K., Foreman, B., 2013. Far-traveled latest Cretaceous-Paleocene conglomerates of the Southern Rocky Mountains, USA: Record of transient Laramide tectonism. GSA Bulletin 125, 490–498, doi: 10.1130/B30699.1.

Huntington, K. W., Wernicke, B. P., Eiler, J. M., 2010. The influence of climate change and uplift on Colorado Plateau paleotemperatures from carbonate clumped-isotope thermometry. Tectonics 29 (TC3005), doi: 10.1029/2009TC002449.

Karlstrom, K. E., Coblentz, D., Dueker, K., Ouimet, W., Kirby, E., Van Wijk, J., et al;, and the CREST working group, 2012. Mantle-driven dynamic uplift of the Rocky Mountains and Colorado Plateau and its surface response: Toward a unified hypothesis. Lithosphere, 4, 3-22.

Landman R. L. and Flowers R. M., 2013. (U-Th)/He thermochronologic constraints on the evolution of the northern Rio Grande Rift, Gore Range, Colorado, and implications for rift propagation models. Geosphere. 9, 170–187, doi:10.1130/GES00826.1

Lague, D., 2010. Reduction of long- term bedrock incision efficiency by short- term alluvial cover intermittency. Journal of Geophysical Research: Earth Surface, 115(F2), 10.1029/2008JF001079

Leonard, E. M., 2002. Geomorphic and tectonic forcing of late Cenozoic warping of the Colorado piedmont. Geology 30, 595–598.

Manners, H. R., Grimes, S. T., Sutton, P. A., Domingo, L., Leng, M. J., Twitchett, R. J., Hart, M. B., Dunkley Jones, T., Pancost, R. D., Duller, R., Lopez-Martinez, N., 2013. Magnitude and profile of organic carbon isotope records from the Paleocene - Eocene Thermal Maximum: Evidence from northern Spain. Earth and Planetary Science Letters 376, 220–230, doi: 10.1016/j.epsl.2013.06.016.

Marr, J. G., Swenson, J. B., Paola, C., & Voller, V. R., 2000. A two- diffusion model of fluvial stratigraphy in closed depositional basins. Basin Research, 12(3- 4), 381-398.

McMillan, M. E., Angevine, C. L., Heller, P. L., 2002. Postdepositional tilt of the Miocene-Pliocene Ogallala Group on the western Great Plains: Evidence of late Cenozoic uplift of the Rocky Mountains. Geology 30, 63–66.

McMillan, M. E., Heller, P. L., Wing, S. L., 2006. History and causes of post-Laramide relief in the Rocky Mountain orogenic plateau. GSA Bulletin 118, 393–405, doi: 10.1130/B25712.1.

McMillan, N. J., Alan, P. D., Haag, D., 2000. Evolution of magma source regions in teh Rio

Grande Rift, southern New Mexico. GSA Bulletin 112, 1582–1593.

Métivier, F., 1999. Diffusive like buffering and saturation of large rivers. Physical Review E 60, 5827–5832.

Métivier, F and Gaudemer, Y., 1999. Stability of output fluxes of large rivers in South and East Asia during the last 2 million years: implications on flood plain processes. Basin Research, 11, 293-303.

Miller, D.A. and White R. A., 1998. A Conterminous United States Multi-Layer Soil Characteristics Data Set for Regional Climate and Hydrology Modeling. Earth Interactions, 2

Mitrovica, J. X., Beaumont, C., Jarvis, G. T., 1989. Tilting of continental interiors by the dynamical effects of subduction. Tectonics 8, 1079–1094.

Mitrovica, J. X., Forte, A. M., 1997. Radial profile of mantle viscosity: Results from the joint inversion of convection and postglacial rebound observables. Journal of Geophysical Research 102, 2751–2769.

Nereson, A., Stroud, J., Karlstrom, K., Heizler, M., McIntosh, W., 2013. Dynamic topography of the western Great Plains: Geomorphic and Ar/ Ar evidence for mantle-driven uplift associated with Jemez lineament of NE New Mexico and SE Colorado. Geosphere 9, 521–545, doi: 10.1130/GES00837.1.

Paola, C., Heller, P. L., Angevine, C. L., 1992. The large-scale dynamics of grain-size variation in alluvial basins, 1: Theory. Basin Research 4, 73–90, doi: 10.1111/j.1365-2117.1992.tb00145.x.

Paola, C., Seal, R., 1995. Grain-size patchiness as a cause of selective deposition and downstream fining. Water Resources Research 31, 1395–1407, doi: 10.1029/94WR02975.

Pelletier, J; D., 2011. Fluvial and slope wash erosion of soil mantled landscapes: detachment or transport limited? Earth Surface Processes and Landforms, 37, 37-51, doi: 10.1002/esp.2187

Pinet, P., Souriau, M., 1988. Continental erosion and large-scale relief. Tectonics 7, 563–582.

Poag and Sevon, 1989. A record of Appalachian Denudation in Postrift Mesozoic and Cenozoic sedimentary deposits of the U.S. middle Atlantic continental margin. Geomorphology 2, 119–157.

Schmitz, B., Pujalte, V., 2007. Abrupt increase in seasonal extreme precipitation at the Paleocene-Eocene boundary. Geology 35, 215–218, doi: 10.1130/G23261A.1.

Simpson, G., Schlunneger, F., 2003. Topographic evolution and morphology of surfaces

evolving in response to coupled fluvial and hillslope sediment transport. Journal of Geophysical Research 108 (B62300).

Sinclair, H. D., Coakley, B. J., Allen, P. A., Watts, A. B., 1991. Simulation of foreland basin stratigraphy using a diffusion-model of mountain belt uplift and erosion - an example from the central Alps, Switzerland. Tectonics 10, 599–620, doi: 10.1029/90TC02507.

Sklar, L. S., and Dietrich, W. E., 2001. Sediment and rock strength controls on river incision into bedrock. Geology, 29, 1087-1090.

Sloss, L. L. 1963. Sequences in the cratonic interior of North America. GSA Bulletin, 74, 93-114.

Smith, T. R., Bretherton, F. P., 1972. Stability and conservation of mass in drainage basin evolution. Water Resources Research 8, 1506–1529, doi: 10.1029/WR008i006p01506.

Spasojevic, S., Liu, L., Gurnis, M., Müller, R. D., 2008. The case for dynamic subsidence of the US east coast since the Eocene. Geophysical Research Letters 35 (L08305), doi: 10.1029/2008GL033511.

Swinehart, J.B., and Diffendal, R.F., 1995, Geologic map of Morrill County, Nebraska and Colorado, U.S. Geological Investigation Series MAP I-2496: U.S. Geological Survey, U.S. Department of the Interior, scale 1:62,500.

Swinehart, J.B., and Diffendal, R.F., 1997, Geologic map of the Scottsbluff 1° x 2° quadrangle, Nebraska and Colorado, U.S. Geological Investigation Series MAP I-2545:

Swinehart, J. B., Souders, V. L., DeGraw, H. M., Diffendal, R. F., 1985. Cenozoic paleogeography of western Nebraska. In: Flores, R. M., Kaplan, S. S. (Eds.), Cenozoic paleogeography of west-central United States. Vol. 3. Society of Economic Paleontologists and Mineralogists (SEPM) Rocky Mountain Section, Denver, Colorado, USA, pp. 209–229.

Tucker, G. E., van der Beek, P., 2013. A model for post-orogenic development of a mountain range and its foreland. Basin Research 24, 241–259, doi: 10.1111/j.1365-2117.2012.00559.x.

Walford, H.L., White N. J. and Sydow J.C., 2005. Solid sediment load history of the Zambezi Delta. Earth and Planetary Science Letters 238, 49–63, doi: 10.1016/j.epsl.2005.07.014.

Watts, A. B., Karner, G. D., Steckler, M. S., 1982. Lithospheric flexure and the evolution of sedimentary basins. Philosophical Transactions of the Royal Society, A 305, 249–281, doi: 10.1098/rsta.1982-0036.

Willett, S. D., Chapman, D. S., Neugebauer, H. J., 1985. A thermo-mechanical model of continental lithosphere. Nature 314, 520–523.

Wisniewski, P. A., Pazzaglia, F. J., 2002. Epeirogenic controls on Canadian River incision and landscape evolution, Great Plains of northeastern New Mexico. The Journal of Geology 110, 437–456, doi: 10.1086/340411.

Wobus, C. W., Tucker, G. E., Anderson, R. S., 2010. Does climate change create distinctive patters of landscape incision? Journal of Geophysical Research 115 (F04008), doi: 10.1029/2009JF001562.

Figure 1
Click here to download Figure: FIGURE-1.pdf

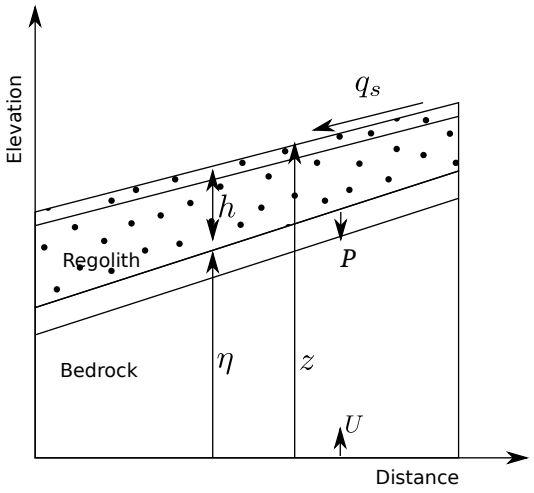

Figure 2
Click here to download Figure: figure2.pdf

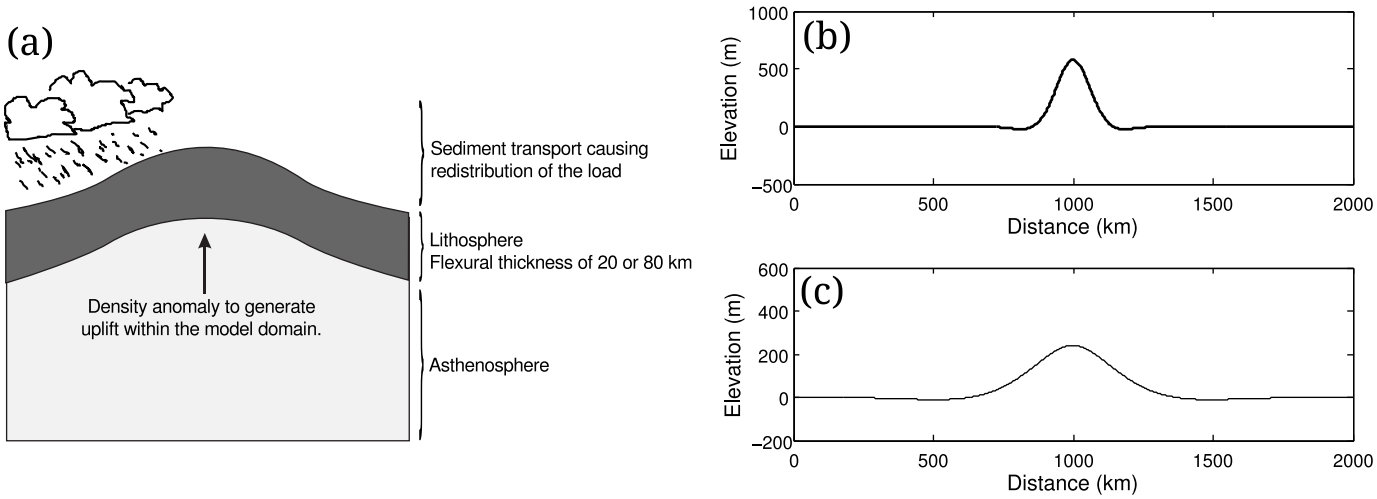

Figure 3
Click here to download Figure: figure3.eps

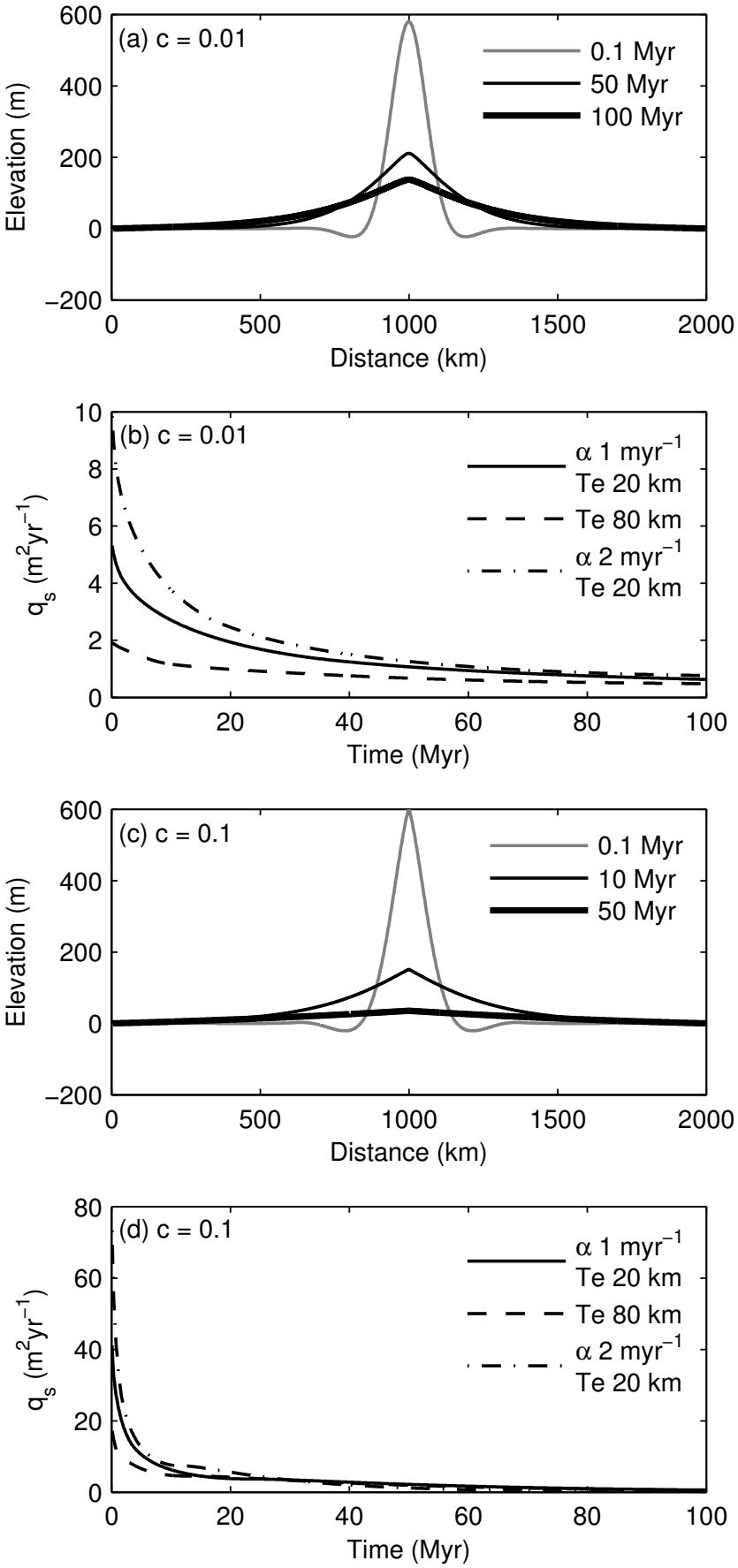

Figure 4
Click here to download Figure: figure4.eps

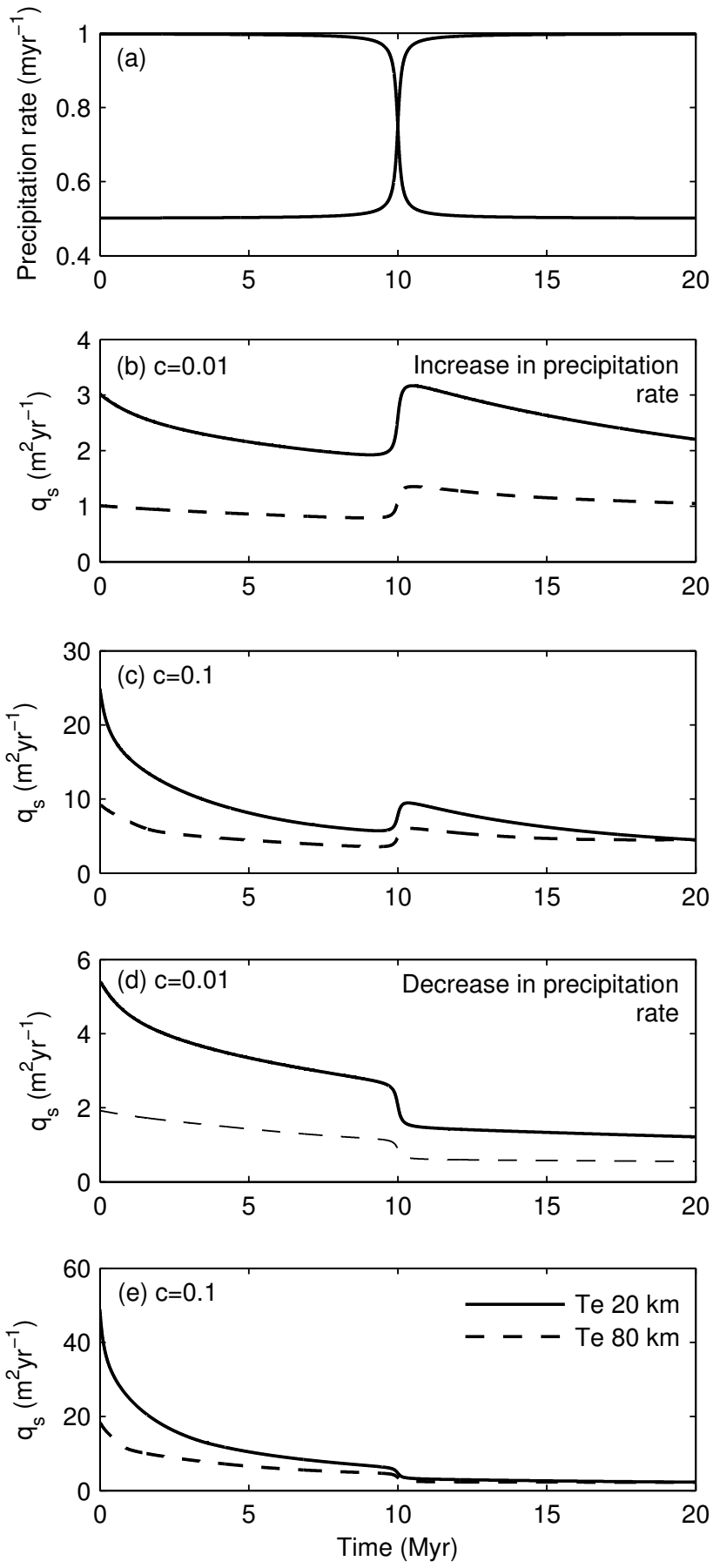

Figure 5
Click here to download Figure: figure5.eps

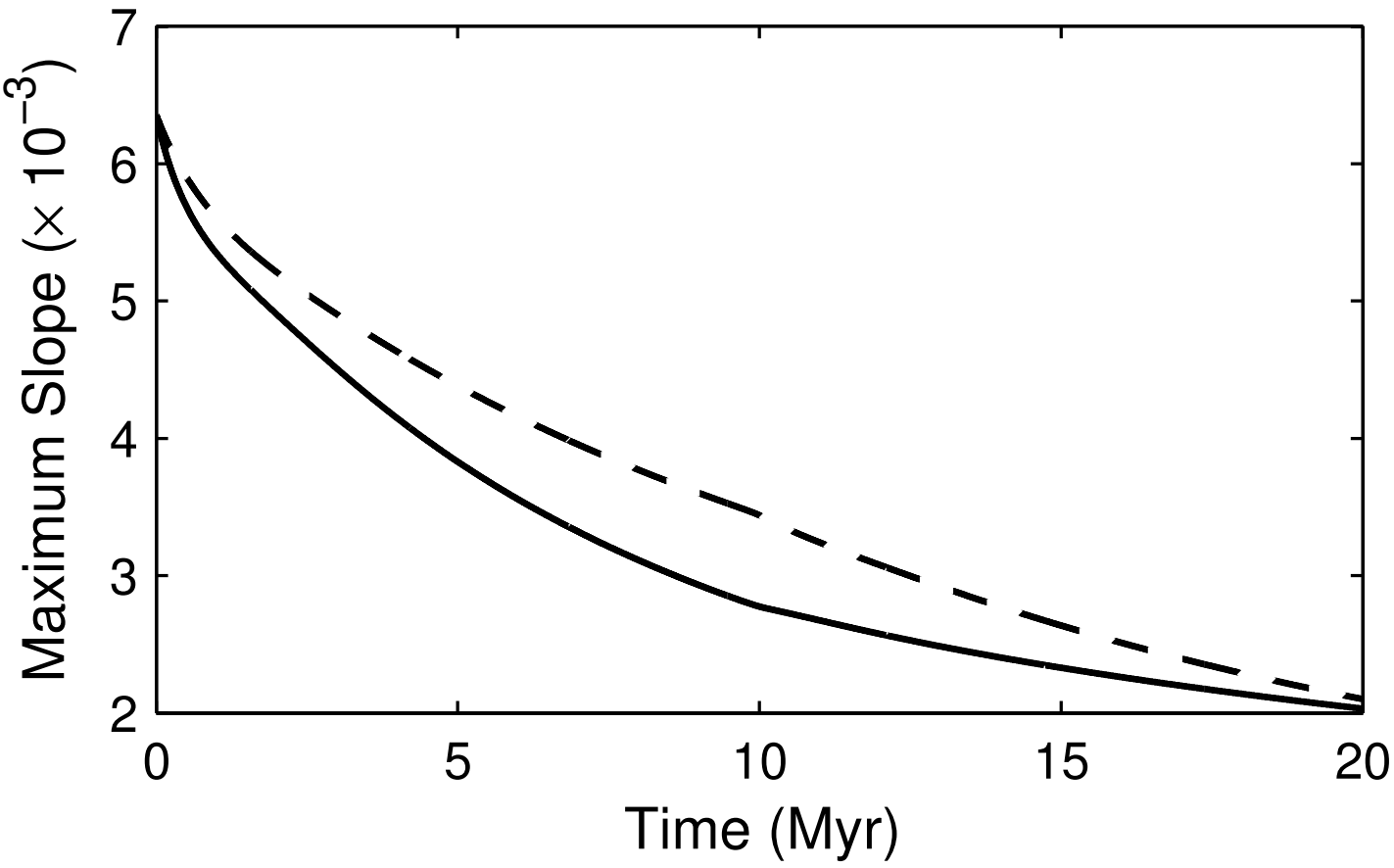

Figure 6
Click here to download high resolution image

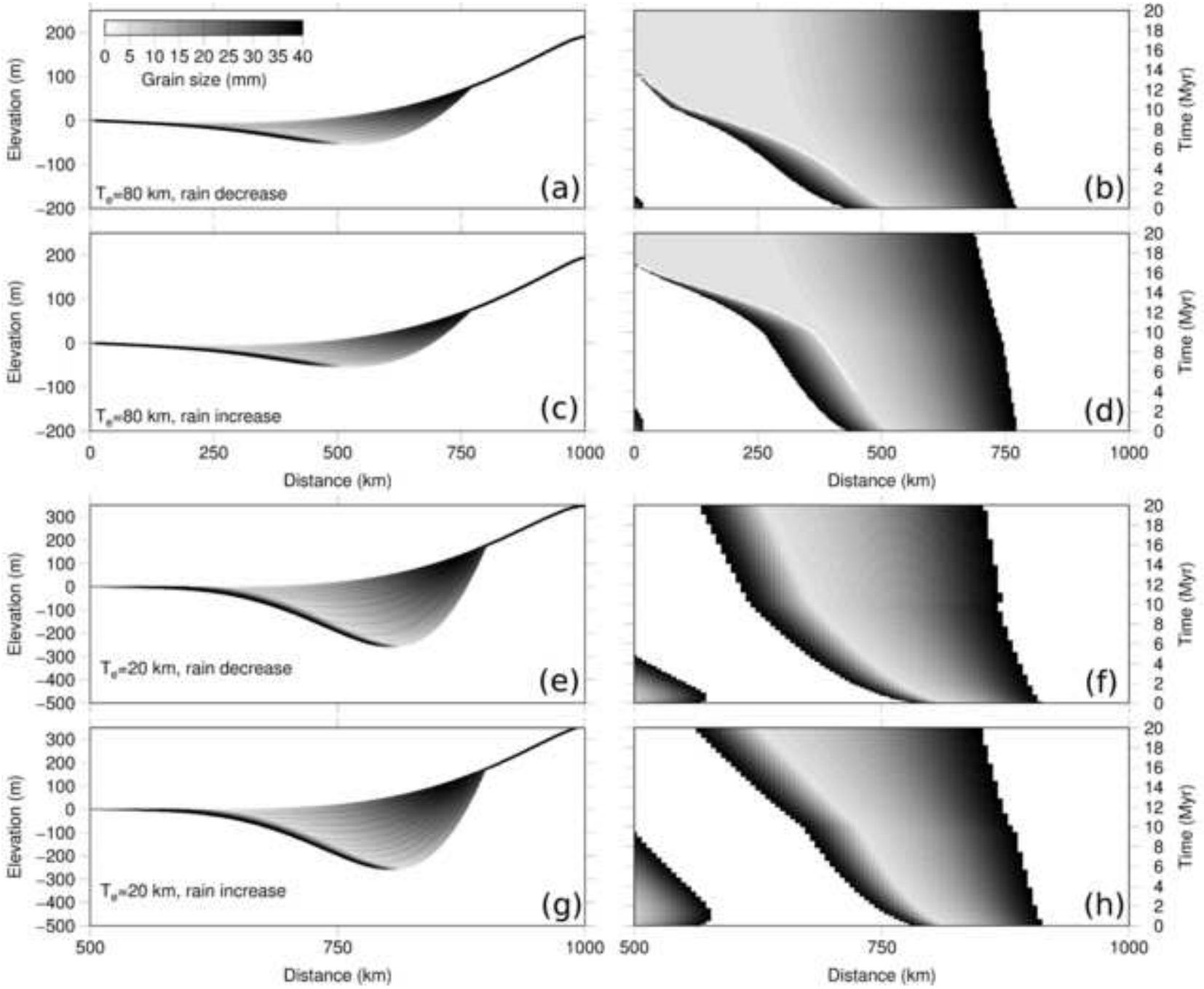

Figure 7
Click here to download high resolution image

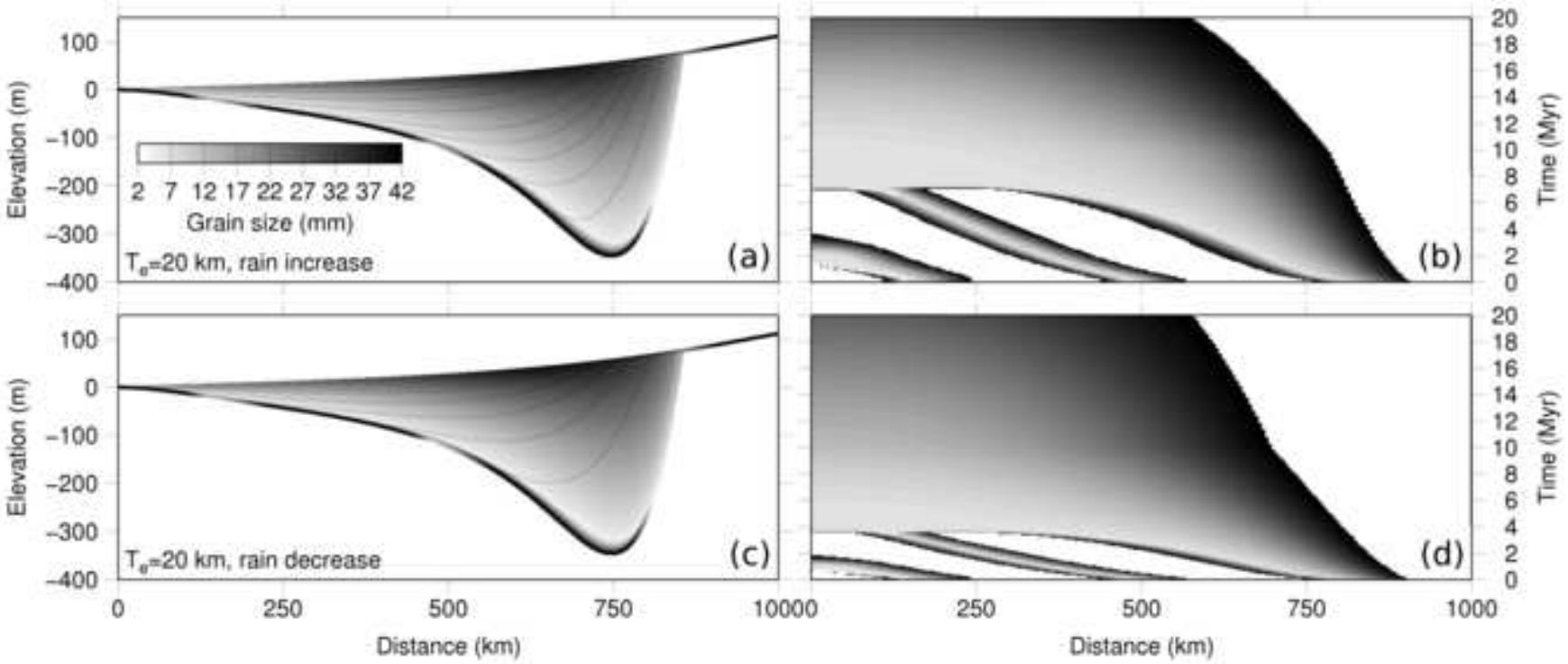

Figure 8
Click here to download Figure: figure8.eps

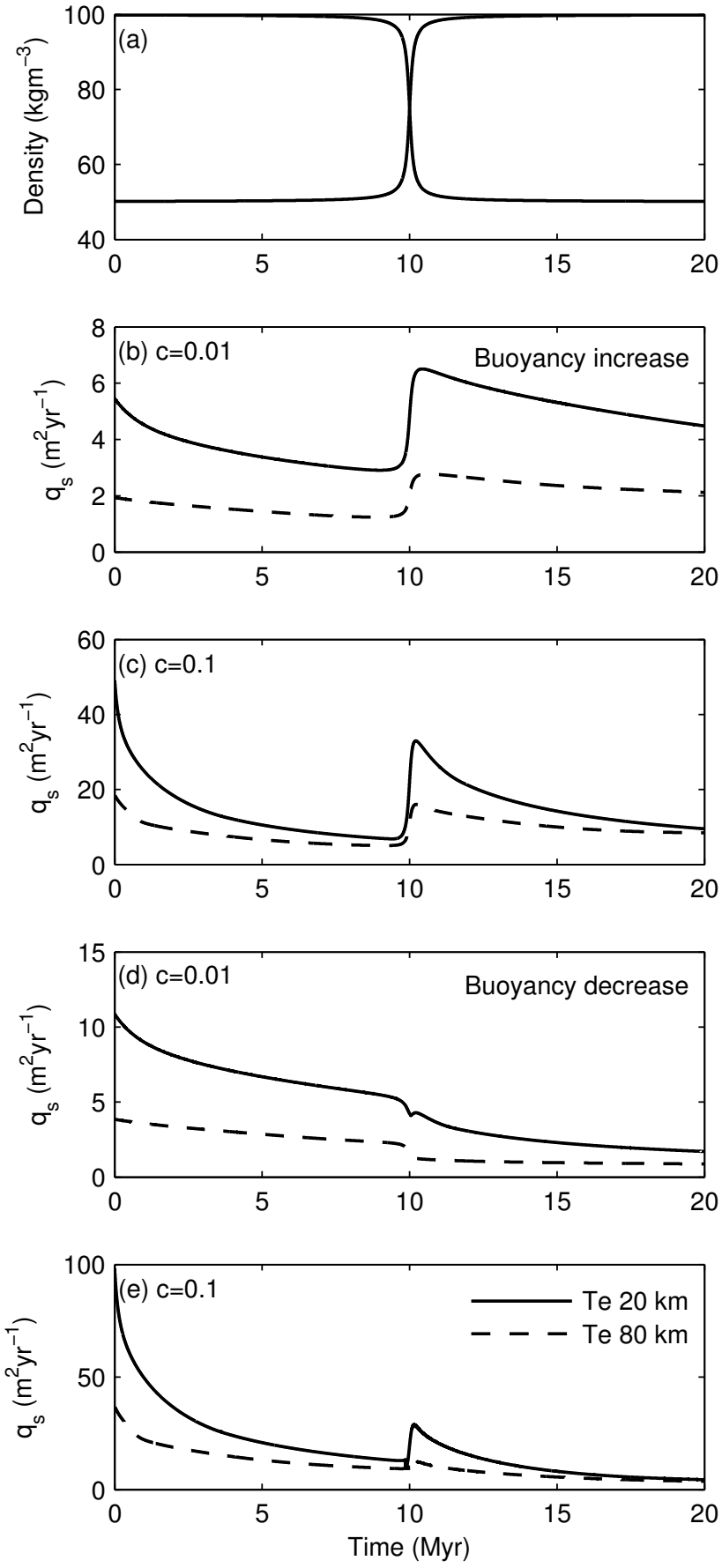

Figure 9
Click here to download Figure: figure9.eps

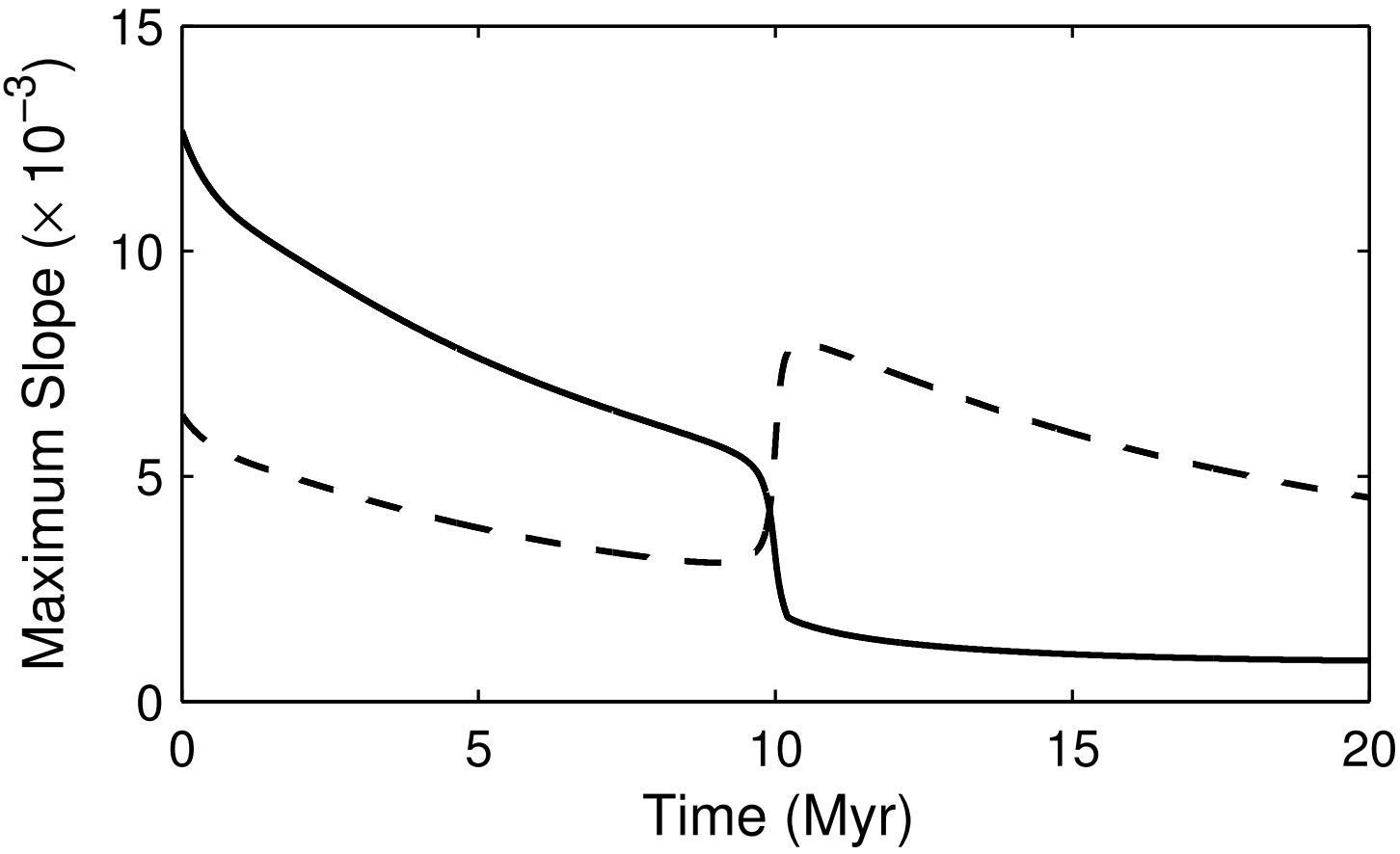

Figure 10
Click here to download Figure: figure10.eps

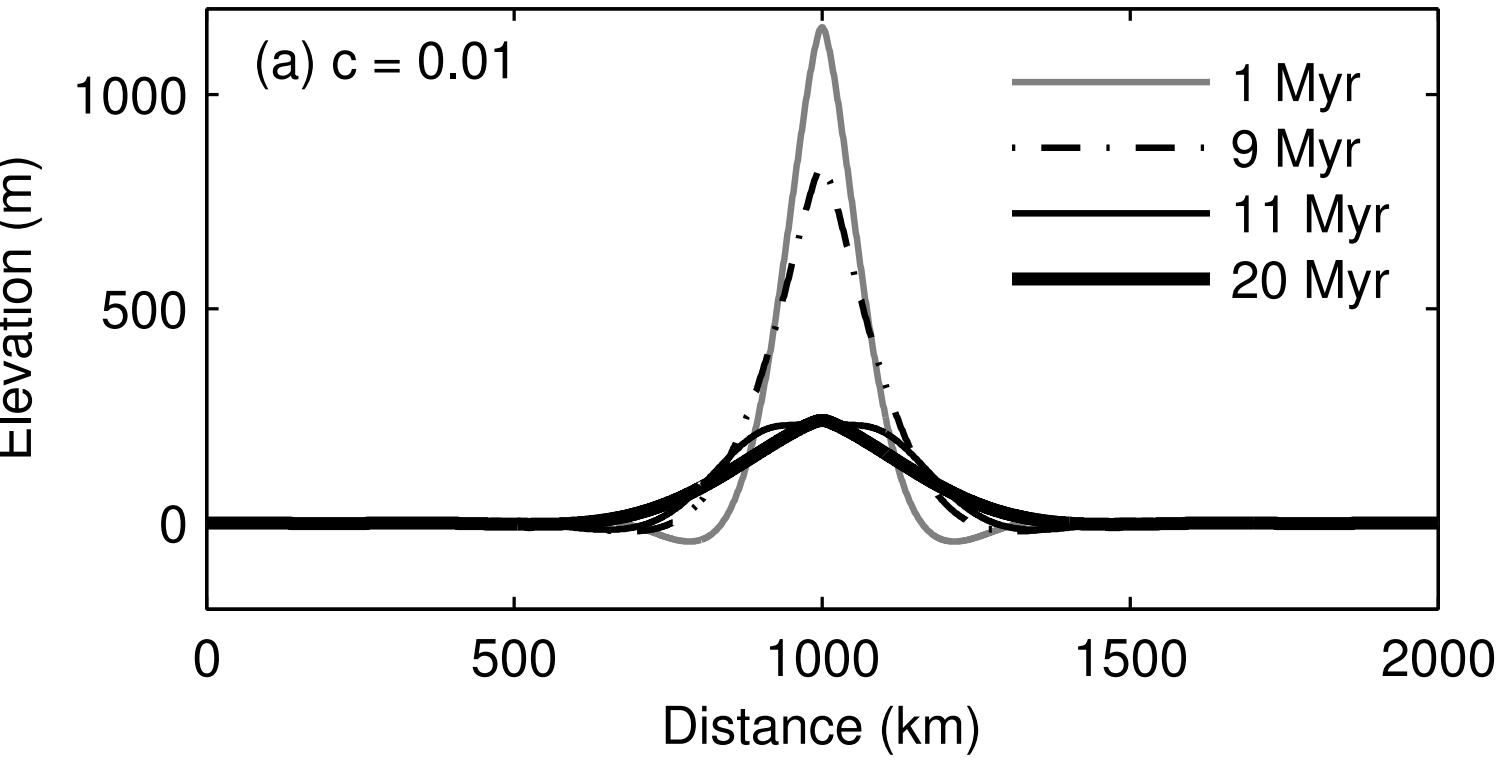

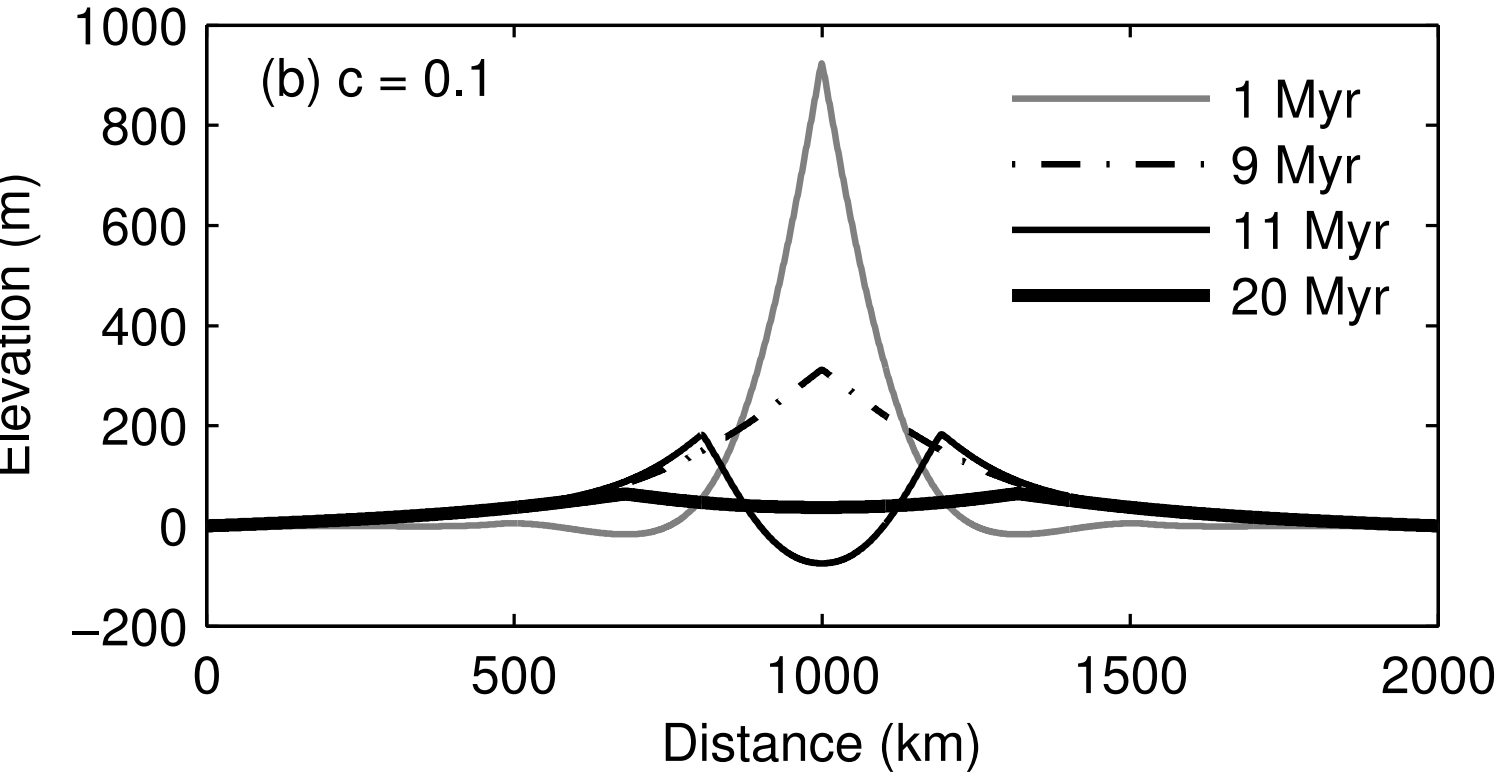

Figure 11
Click here to download high resolution image

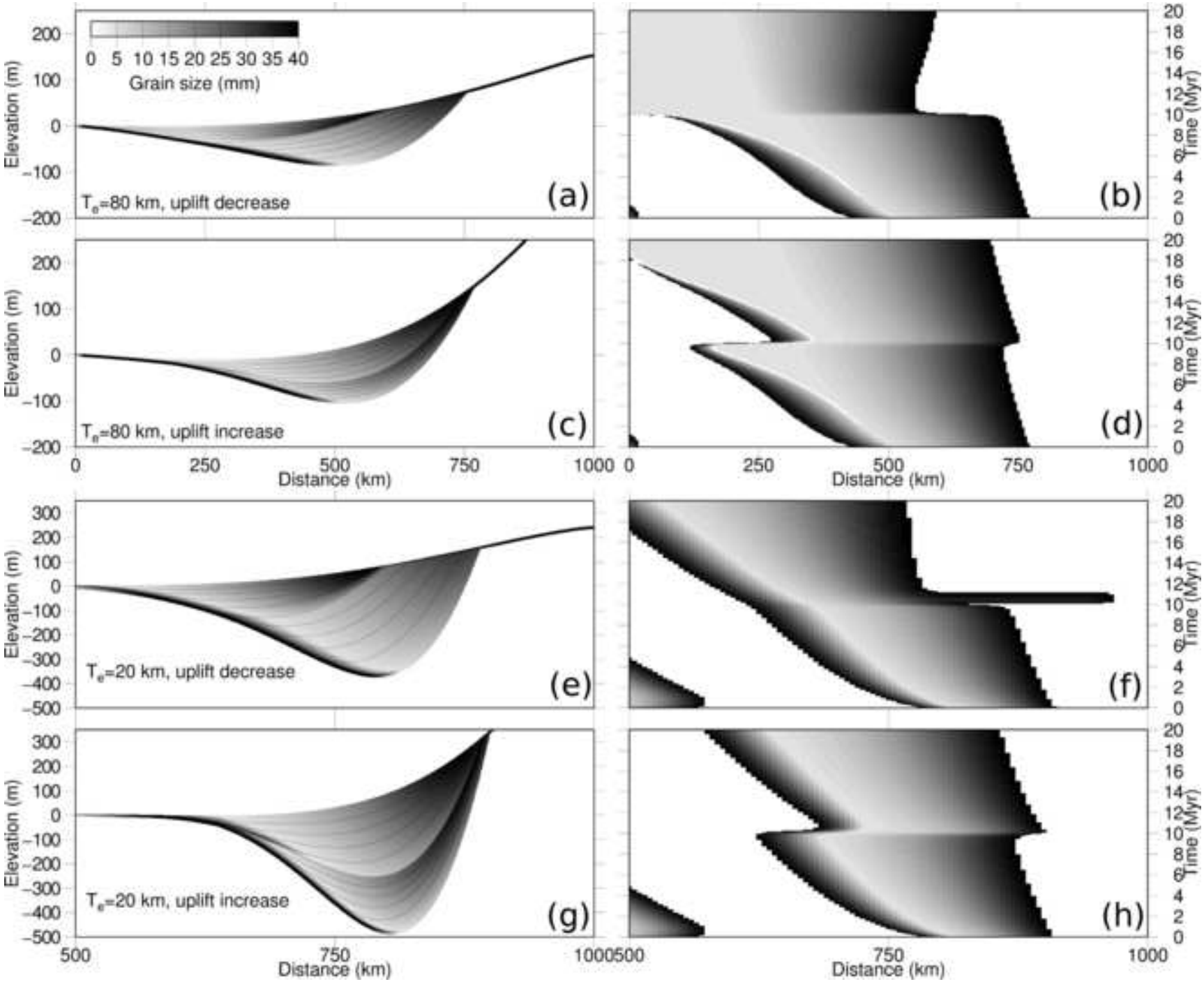

Figure 12
Click here to download high resolution image

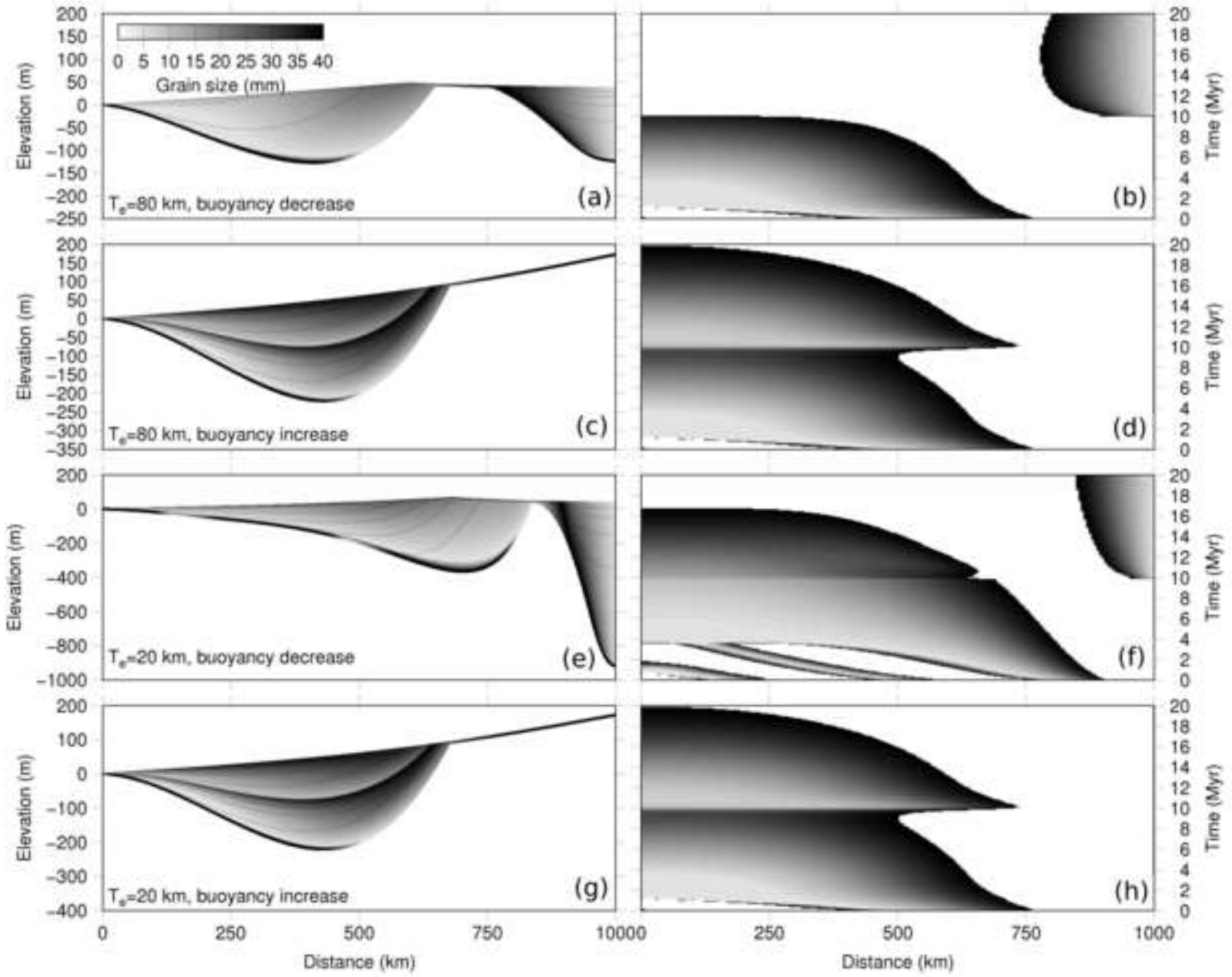

Figure 13
Click here to download Figure: figure13.pdf

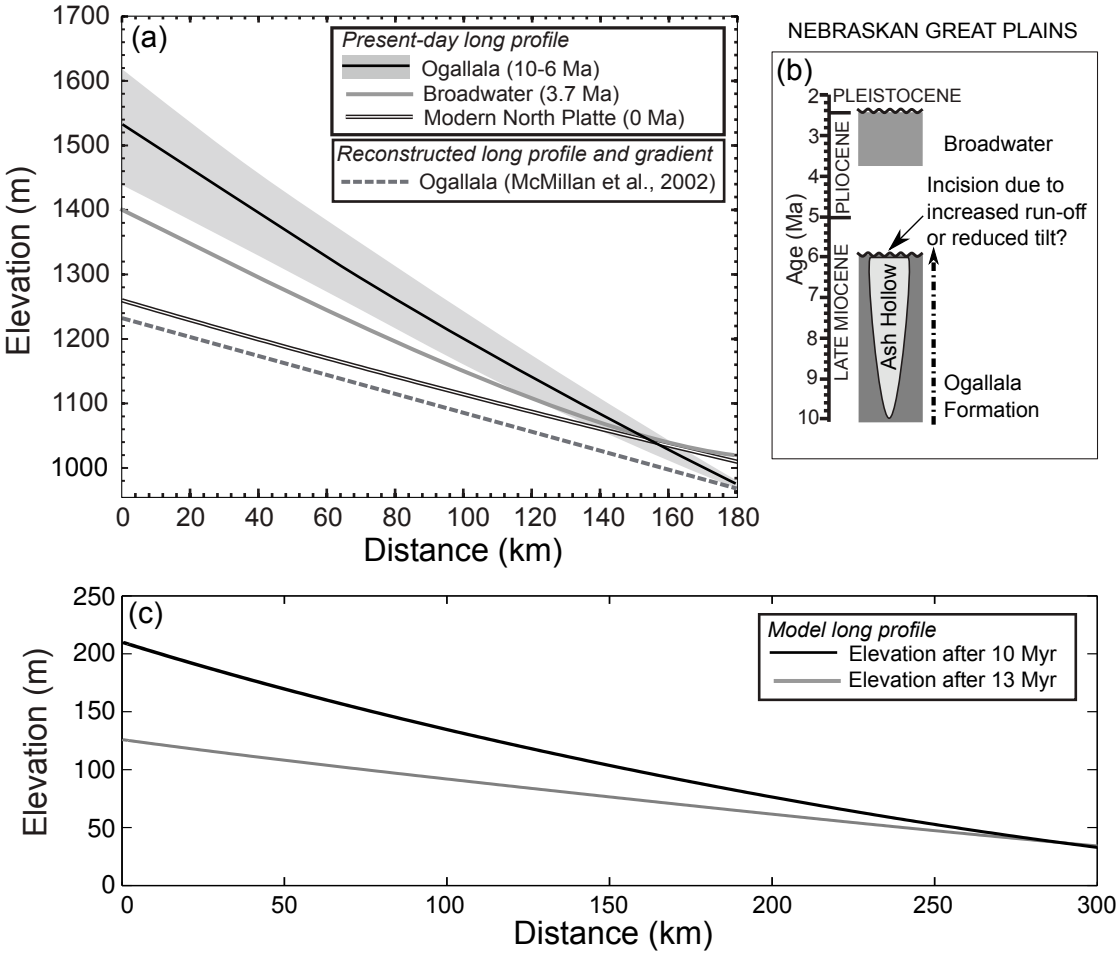

Table 1: Model parameters and assumed values

Variable	Meaning and Units	Value
A	Non-dimensional constant to account for meandering or braided river.	1 or 0.15
c	Fluvial transport coefficient	1×10^{-2}
C_0	Volume concentration of sediment in the bed	0.7
C_f	Dimensionless drag coefficient	0.01
C_g	Relative partitioning of the variance in the gravel supply into down-system change in standard deviation (see Fedele and Paola, 2007; Duller et al., 2010)	0.7
C_V	Coefficient of variation (see Fedele and Paola, 2007)	0.25
D_f	Flexural rigidity, Nm	
D_e	Ratio of non-fluvial versus fluvial coefficients of transport	
D_{50}	Median input grain size, mm	40
D_{84}	84th percentile of input grain size distribution, mm	70
$\bar{D}$	Mean of the $\log_{10}$ of the deposited grain size	
$\bar{D}_0$	$\log_{10}$ of the median input grain size	
E	Young's modulus, Pa	1×10^{11}
g	Acceleration due to gravity, ms^{-1}	9.81
h	Thickness of regolith layer (Figure 1), m	
L	Length of model domain, m	2×10^{6}
p	Imposed load on the lithosphere, Pa	
P	Production of regolith (Figure 1), myr^{-1}	
q_s	Sediment flux, myr^{-1}	
q_w	Water flux, m^2yr^{-1}	
r	Dimensionless distribution of deposition down-system (see Paola and Seal, 1995)	
s	Specific gravity of sediment	2.7
T_e	Elastic thickness, m	20 or 80×10^{3}
U	Rock uplift (Figure 1), myr^{-1}	
w	Displacement due to flexure of the lithosphere, m	
$\tilde{x}_d$	Dimensionless down-system deposition length	

$\tilde{y}_d$	Spatial transformation of $\tilde{x}_d$	
α	Precipitation rate, myr^{-1}	
κ	Linear diffusion coefficient, m^{2}yr^{-1}	1×10^2
ρ_m	Mantle density, kgm^{-3}	3300
ρ_{fill}	Density of material deposited, equal to crustal density, kgm^{-3}	2700
φ_0	Grain size variance	
ν	Diffusion coefficient for sediment transport, m^{2}yr^{-1}	
ν_p	Poisson's ratio	0.25